Progress in Oceanography 173 (2019) 134–164

Contents lists available at ScienceDirect

Progress in Oceanography

journal homepage: www.elsevier.com/locate/pocean

Artificial evolution of behavioral and life history strategies of high-latitude copepods in response to bottom-up and top-down selection pressures

Kanchana Bandara[a,b,*], Øystein Varpe[b,c], Rubao Ji[d], Ketil Eiane[a]

[a] Faculty of Biosciences and Aquaculture, Nord University, 8049 Bodø, Norway
[b] The University Centre in Svalbard, 9171 Longyearbyen, Norway
[c] Akvaplan-niva, Fram Centre, 9296 Tromsø, Norway
[d] Woods Hole Oceanographic Institution, Redfield 2-14, Woods Hole, MA 02543, USA

ARTICLE INFO

Keywords:
Seasonality
Life history evolution
Vertical migration
Arctic
Calanus
Optimization model

ABSTRACT

Strong seasonality of resources and predation risk act as bottom-up and top-down selection pressures in high-latitudes, under which numerous behavioral and life history strategies evolve. Although such seasonal strategies are well-documented among high-latitude marine zooplankton, it is difficult to separate the role of bottom-up and top-down selection pressures in the evolution of seasonal strategies. Here, we present a model that allows partitioning of bottom-up (i.e. food availability and temperature) and top-down (i.e. visual predation risk) selection pressures to study how behavioral and life history strategies of high-latitude copepods evolve. In the model, timing, amplitude and ontogenetic trajectories of diel and seasonal vertical migrations (DVM and SVM) were defined as behavioral strategies. Body size, generation time and birth time comprised the life history strategy. Numerous combinations of behavioral and life history strategies were hardwired to copepods representing three model species. In a given model environment, strategies were evaluated for growth, survival and reproductive performances using a fitness estimate, which was heuristically maximized using a Genetic Algorithm. Model simulations were performed in three seasonality regimes representing various levels of visual predation risk from low- to high-Arctic. At lower visual predation risk, species-specific behavioral and life history strategies were largely influenced by food availability and temperature. As visual predation risk increased, the influence of bottom-up selection pressures diminished, and irrespective of the modelled latitude, all model species employed largely similar strategies to counter the predation risk. Modest increase of visual predation risk stimulated the diel vertical migration behavior. Further increase of visual predation risk was associated with decrease of body size, which created a significant impact on the observed behavioral and life history strategies through allometric processes. Our findings suggest that top-down selection pressures play a significant role in the evolution of behavioral and life history strategies of high-latitude copepods.

1. Introduction

High-latitude pelagic environments are characterized by strong seasonal oscillations of irradiance, which drives seasonal patterns of temperature, primary production and predation risk. These impose strong bottom-up and top-down selection pressures on pelagic inhabitants (Hunter and Price, 1992; Power, 1992; Varpe, 2017) and result in a wide range of behavioral and life history adaptations (McLaren, 1966; Ohman, 1988; Conover, 1992; Szulkin et al., 2006; Williams et al., 2017). Seasonal adaptations are usually linked with trade-offs, as all adaptive traits cannot be simultaneously improved without compromising each other, especially in seasonally resource-limited environments with elevated predation risk (Stearns, 1989; Fabian and Flatt, 2012; Varpe, 2017).

Seasonal behavioral and life history adaptations and associated trade-offs are well-documented among marine zooplankton, and especially among the herbivore community (reviewed in Conover and Siferd, 1993; Hagen and Auel, 2001; Varpe, 2012). These involve adaptations to cope with both the productive and unproductive parts of the year. During the productive season (spring–summer), zooplankton tend to feed in the warmer, food-rich, near-surface waters to grow and develop rapidly toward attaining sexual maturity (Hopkins et al., 1984; Huntley and Lopez, 1992; Lee et al., 2003; Escribano et al., 2014). However, residing in surface waters elevates the mortality risk through visual predation. This is usually countered by diel vertical migration (DVM), which is a behavioral strategy that trades off growth potential

* Corresponding author at: Faculty of Biosciences and Aquaculture, Nord University, 8049 Bodø, Norway.
E-mail address: kanchana.bandara@nord.no (K. Bandara).

https://doi.org/10.1016/j.pocean.2019.02.006
Received 25 April 2018; Received in revised form 21 January 2019; Accepted 7 February 2019
Available online 08 February 2019

for survival (Lampert, 1989; Loose and Dawidowicz, 1994; Hays, 2003). Further, structural growth of late developmental stages of many high-latitude zooplankton is traded off to build up energy reserves (Lee et al., 2006). Such trade-offs together with shorter productive season and seasonal peaks of visual predation risk usually makes it difficult and/or sub-optimal for relatively large zooplankton to attain sexual maturity and reproduce within the same calendar year (Hirche, 1996b; Hagen, 1999; Kaartvedt, 2000; Varpe and Fiksen, 2010). Instead, as the unproductive season (autumn–winter) approaches, zooplankton perform seasonal vertical migrations (SVM) to deeper waters and overwinter with minimal biological activity (i.e. diapause, Carlisle and Pitman, 1961; Hirche, 1996a).

The inability to maintain high biological activity during the unproductive part of the year tends to increase the generation time (Conover, 1988; Falk-Petersen et al., 2009) and consequently elevates body sizes of most high-latitude zooplankton (Hall et al., 1976; Gillooly et al., 2002). Further, as generation time and body size tend to relate inversely with temperature, a generic south to north trend (increase) in these traits can be predicted from lower- to higher-Arctic locations (see Rohde, 1992; Blackburn et al., 1999). However, since both these traits show plasticity to top-down selection pressures (Brooks and Dodson, 1965; Gillooly, 2000; Jeppesen et al., 2004), it is interesting to investigate how growth and reproductive advantages of a longer lifespan and larger body size (McLaren, 1966) are traded off for survival at elevated levels of size-dependent predation risk. In addition, as body size dynamics (influenced by bottom-up or top-down selection pressures) can directly influence physiological and behavioral activity through allometric relationships (Brown et al., 2004), it is crucial to study how these processes influence seasonal behavioral and life history adaptations of high-latitude zooplankton.

Predominantly herbivorous zooplankton occupy a crucial trophic position between primary producers and higher-order consumers, and are well-suited for studying the influences of bottom-up and top-down selection pressures (Hays et al., 2005). In the Arctic, three congeners of *Calanus*, i.e. *C. finmarchicus*, *C. glacialis* and *C. hyperboreus* usually dominate the herbivore biomass (Eiane and Tande, 2009). Despite the largely similar morphologies, these three species exhibit diverse behavioral and life history strategies that are plastic to environmental variability (Table 1). Field investigations on the Arctic *Calanus* congeners are limited in their ability to partition the bottom-up and top-down environmental drivers, largely due to difficulties of quantifying and manipulating predation risk. Although laboratory experiments can address this limitation (e.g. Zaret and Suffern, 1976; Bollens and Frost, 1991), it cannot reproduce the space (i.e. depth) and timescales (i.e. multiple generations over seasonal cycles) through which most behavioral and life history strategies evolve. In contrast, theoretical modeling studies have shown promise in their ability to manipulate bottom-up and top-down selection pressures (e.g. Fiksen and Giske, 1995; Fiksen and Carlotti, 1998; Varpe and Fiksen, 2010; Ji et al., 2013b). However, models with simultaneous improvements in spatial, temporal and biological resolution are rare, mainly due to elevated computational demands. Consequently, most life history models of high-latitude zooplankton are either not species-specific or often overlook the behavioral decisions made on daily basis (Bandara et al., 2018).

In this study, we present a high-resolution model (in terms of space, time and species-specificity) of behavioral and life history strategies of Arctic *Calanus* species. In the model, species-specific optimal behavioral and life history strategies are artificially evolved in a deterministic model environment, within which bottom-up (i.e. food availability and temperature) and top-down (i.e. predation risk) selection pressures are manipulated. By performing model simulations along environmental gradients that offer varying levels of food availability, temperature and predation risk, we aim to investigate (i) the dominant driver of behavioral and life-history strategies of high-latitude copepods, and (ii) the species-specific behavioral and life-history strategies that evolve along the modelled environmental gradients.

2. Materials and methods

2.1. Model overview

The present model is an extension of our previous work Bandara et al. (2018), in which we presented a high-resolution model that allows artificial evolution of diel and seasonal vertical migratory strategies of high-latitude copepods. However, the above model was based on a generic high-latitude copepod with a fixed body size and a generation time of one year. Therefore, we designed the present model to relax the key assumptions of Bandara et al. (2018) by (i) making the model species-specific, (ii) allowing plasticity of body size and generation times and (iii) making improvements to the growth, survival and reproduction submodels.

The model consists of three entities: strategies, model organism and the model environment (Section 2.2.1). Strategies are pre-defined diel and seasonal behavioral patterns and life history attributes hardwired to the model organism (Fig. 1, Table 2). The model organism represents copepods belonging to three model species that represent high-latitude

Table 1
The inter-and intra-specific diversity of some life history traits/attributes of *Calanus* spp. Body mass estimates (adult stages) are from prosome length (PL) to dry mass (DM) relationships published by Robertson (1968). Cited literature only serve as examples. See Falk-Petersen et al. (2009), and Bandara (2014) for an extensive review on some of these life history traits.

Trait/attribute	*C. finmarchicus*	*C. glacialis*	*C. hyperboreus*
Center of distribution	North Atlantic[5,11]	Arctic (shelf) [5,11]	Arctic (oceanic) [11]
Body size			
Length (mm PL)	2.2[4]–3.2[14,30,17]	3.0[14,17,25]–4.6[17,28]	3.9[17]–6.7[28]
Mass (μg DM)	204–557[3]	533–1742[3]	1016–5947[3]
Timing of reproduction	In synchrony with pelagic bloom[8,16,31]	Before or in synchrony with pelagic bloom[12,22,26,32]	Before the pelagic bloom[6,7,12,26]
Reproductive strategy	Income breeding[18]	Income or capital breeding[32]	Capital breeding[2,19]
Most common overwintering stages	CIV[8,31,33] CV[15,22,28]	CIV[23,17,29] CV[13,21,24]	CIII[13,27] CIV[6,7,29] CV[20,25,28] Females[13,21,29]
Most common generation times (years)	1[9,21,29]	1–2[10,23,24,29]	1–3[1,13,20,23,25]

[1] Conover (1965), [2] Conover (1967), [3] Robertson (1968), [4] Jaschnov (1972), [5] Fleminger and Hulsemann (1977), [6] Dawson (1978), [7] Matthews et al. (1978), [8] Tande and Hopkins (1981), [9] Aksnes and Magnesen (1983), [10] Tande et al. (1985), [11] Conover (1988), [12] Smith (1990), [13] Hirche (1991), [14] Unstad and Tande (1991), [15] Diel and Tande (1992), [16] Plourde and Runge (1993), [17] Hirche et al. (1994), [18] Hirche (1996b), [19] Hirche and Niehoff (1996), [20] Hirche (1997), [21] Hirche and Kwasniewski (1997), [22] Melle and Skjoldal (1998), [23] Falk-Petersen et al. (1999), [24] Scott et al. (2000), [25] Madsen et al. (2001), [26] Niehoff et al. (2002), [27] Astthorsson and Gislason (2003), [28] Hirche and Kosobokova (2003), [29] Arnkværn et al. (2005), [30] Daase and Eiane (2007), [31] Madsen et al. (2008), [32] Søreide et al. (2010), [33] Hirche and Kosobokova (2011).

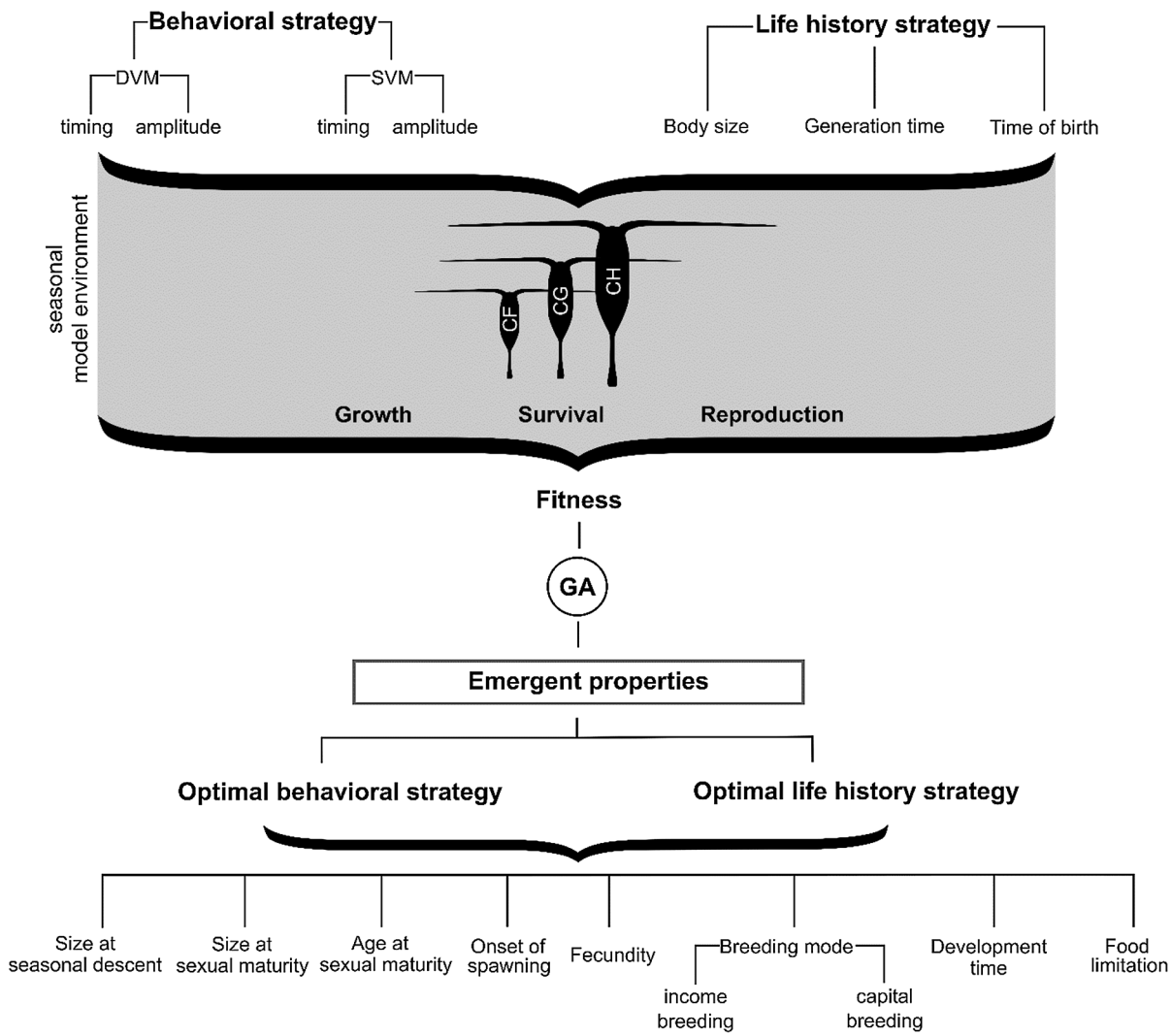

Fig. 1. The model overview. The behavioral strategy (vertical strategy) and some key aspects of the life history strategy are defined by seven evolvable free parameters (cf. Table 2). These are hardwired to model copepods of three different species representing *C. finmarchicus*, *C. glacialis* and *C. hyperboreus*. For a given model environment, a Genetic Algorithm heuristically optimize these parameters through a fitness function of growth, survival and reproduction, and predicts the environment- and species-specific optimal behavioral and life history strategies.

Table 2
List of evolvable (soft) parameters optimized by the Genetic Algorithm. The parameters β, δ and ε are proxies that define the behavioral strategy (vertical strategy), while the rest define some key aspects of the life history strategy. These evolvable parameters are hardwired to copepods spawned in different times of the year (t_B).

Term	Definition	Range	Interval	Unit
α	Body size parameter	0–1	0.01	–
β	Irradiance threshold parameter	10^{-7}–1	$\times 10$[a]	μmol m^{-2} s^{-1}
γ	Energy allocation parameter	0–1	0.01	–
δ	Seasonal descent parameter	0–1	0.01	–
ε	Seasonal ascent parameter	0–1	0.01	–
η	Generation time parameter	1–3	1	years
t_B	Birth time[b]	1–8760	1	h

[a] Factor of 10 (i.e. 10^{-7}, 10^{-6}, 10^{-5}, 10^{-4}, 10^{-3}, 10^{-2}, 10^{-1} and 1).
[b] The time of being spawned.

Calanus spp. The model environment is a 1000-m deep one-dimensional seasonal setting parameterized for irradiance, temperature, food availability and predation risk in 1 m spatial resolution.

For a given model species in a given model environment, the model initializes by seeding N ($=2.5 \times 10^6$) eggs into random depths (< 50 m) of the model environment at random times of the year. Each seed is randomly assigned a behavioral and life history strategy that a copepod follows throughout its lifespan, which can last up to three years depending on the model species (Fig. 1, Table 1). Growth and development, survival and reproduction of each copepod is simulated in 1 h time intervals (Section 2.2.2). Five state variables are used to trace the vertical position, body mass, size of the energy reserve, fecundity and survivorship throughout the copepod's lifespan. The simulated strategies are evaluated by a fitness measure that integrates the expected lifetime reproduction and survival performances (Section 2.2.3). The fitness is heuristically maximized using a Genetic Algorithm (GA: Holland, 1975) to predict species-and environment-specific optimal behavioral and life history strategies (Section 2.2.4).

2.2. Model description

2.2.1. Entities

2.2.1.1. Strategies. Strategies are of two types: behavioral strategy and life history strategy. The behavioral strategy (i.e. vertical strategy) defines the timing, amplitude and the ontogenetic trajectories of DVM and SVM (Fig. 1). These are represented by three evolvable (soft) parameters. The timing and amplitude of DVM is defined by the

irradiance threshold parameter (β), while those of SVM is defined by the seasonal descent and ascent parameters (δ and ε, Table 2). The life history strategy represents a collection of life history traits (i.e. birth time, body mass, generation length, size at diapause onset, age and size of sexual maturity, onset of spawning, breeding mode and fecundity) and their size- or stage-specific variability (Fig. 1). From these, the birth time, body size and generation length are represented by three evolvable parameters (t_B, α and η: Table 2). Other life history traits emerge as the evolvable parameters are optimized in the model.

2.2.1.2. Model organism. The model organism characterizes hypothetical, semelparous female copepods belonging to three model species: *CF*, *CG* and *CH*. These represent predominantly herbivorous copepods *C. finmarchicus*, *C. glacialis* and *C. hyperboreus* in terms of their body size, behavior and life history strategies. Although these species are distributed throughout the Arctic, only *C. glacialis and C. hyperboreus* are considered as species with a true Arctic origin, where *C. finmarchicus* is a boreal species that primarily inhabit the sub-Arctic and temperate parts of the North Atlantic (Fleminger and Hulsemann, 1977; Conover, 1988). *Calanus* spp. possess a 13-developmental stage ontogeny, which includes an embryonic stage, six naupliar stages (NI–NVI), five copepodite stages (CI–CV) and the sexually mature adult stage. Older developmental stages can store lipids, which act as energy reserves to meet the metabolic demands during diapause (Hirche, 1996a; Hagen and Auel, 2001). However, overwintering stage composition, size of energy reserves and potential diapause duration vary between species (Table 1 and see also, Falk-Petersen et al., 2009; Maps et al., 2013). Reproduction of *Calanus* spp. usually occur in the spring, but the timing and the degree of capital breeding (cf. Varpe et al., 2009) vary between the three species (Table 1). *C. hyperboreus* has the longest life cycle duration (usually 3 years) and largest body size, while the relatively small *C. finmarchicus* and *C. glacialis* usually complete their life cycles within 1 or 2 years (Table 1).

In this model, the model organisms act as carriers of pre-defined behavioral and life history strategies. Although the strategies vary with the ontogeny of the model organism via allometric processes, the model assumes that internal states and individual personalities cannot override the strategies that the model organism follow throughout its lifespan (but see Pedersen et al., 1995; Hays et al., 2005; Kralj-Fišer and Schuett, 2014). This strategy-oriented construct of the model tends to overlook some biological details at individual level, which leads to the lack of population level responses, for instance in response to density dependence. Consequently, the modelled behavioral and life history strategies do no show quantitative feedbacks with the model environment (e.g. impact of grazing on food concentration and duration of the productive season).

2.2.1.3. Model environment. The model runs in three 1000-m deep artificial seasonal environments that roughly represent the expected environmental variability along a latitudinal gradient extending from the north Atlantic to the Arctic (ca. 60–80°N). These model environments do not refer to specific geographic locations, but the modelled environmental

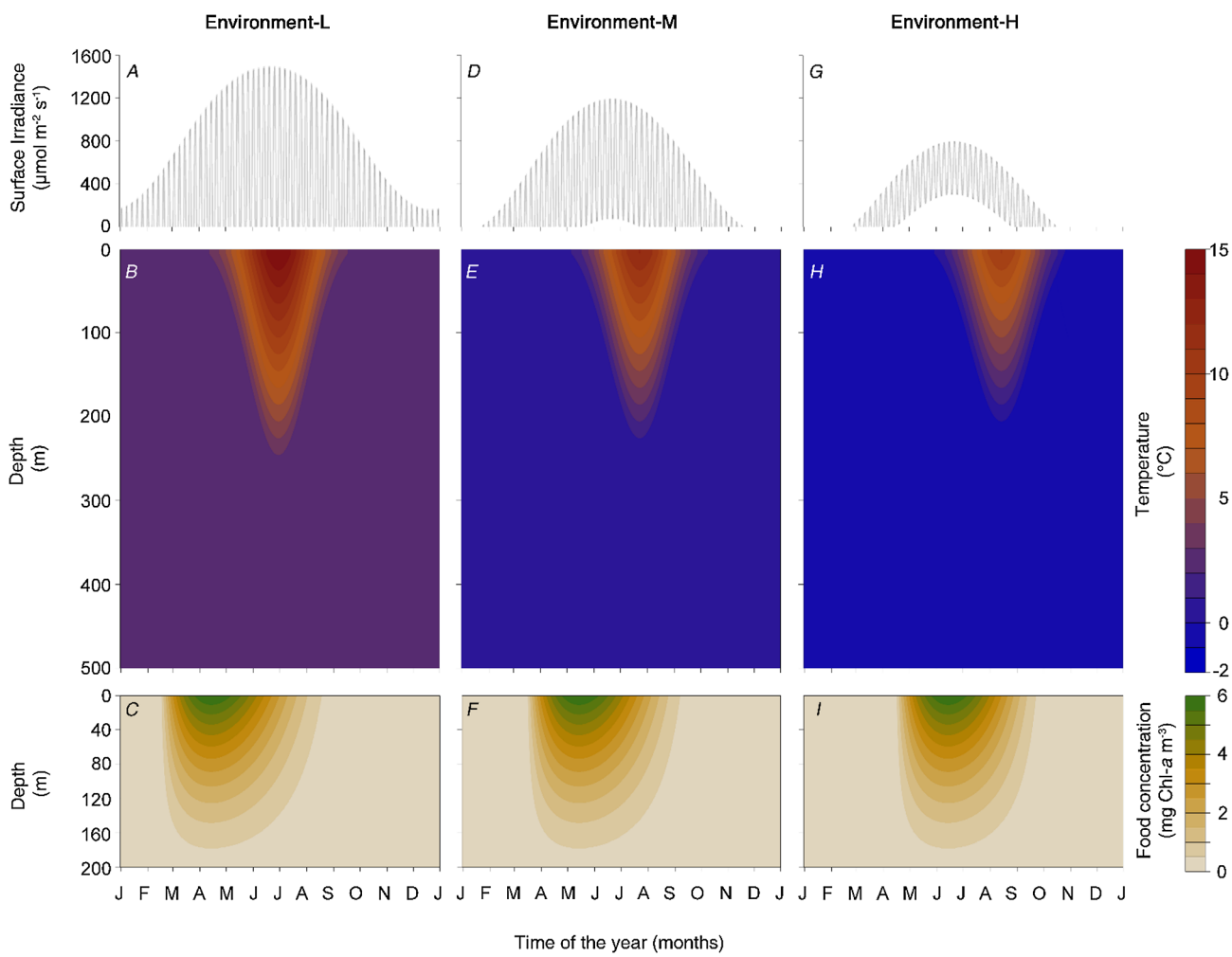

Fig. 2. Dynamics of modelled sea-surface irradiance (A, D, G), temperature (B, E, H) and food availability (C, F, I: as Chlorophyll-a biomass) in the three model environments. The bottom depth is 1000 m, but the ordinates of lower panels are cropped due to the vertical homogeneity of those variables. See Appendix A for a detailed comparison.

variables were adopted from field measurements taken in this region (Appendix A). Since water mass characteristics of this region (e.g. Swift, 1986) were not modelled for simplicity, the model environments represent typical annual oceanographic characteristics of deep Arctic fjords (reviewed in Cottier et al., 2010). The Environment-L characterizes the lower end of the modelled latitudinal gradient (ca. 60°N). Here, the modelled irradiance, temperature and primary production show pronounced seasonal and vertical variability (Fig. 2A–C) but are assumed constant between years. The modelled sea-surface irradiance follows the global clear-sky horizontal irradiance formulations of Robledo and Soler (2000), and peaks at ca. 1500 μmol m^{-2} s^{-1} (Fig. 2A). The modelled temperature peaks at 15 °C in the summer and distributes evenly across the surface mixed layer (Fig. 2B). The depth of the surface mixed layer follows the seasonal pattern described by Mann and Lazier (2006), and reaches a maximum of 500 m during the winter. Below the mixed layer, temperature decreases with depth and converges to a minimum of 2 °C (Fig. 2B). The pelagic primary production extends from mid-February to late-September, with a chlorophyll-*a* peak of 6 mg m^{-3} in mid-April (Fig. 2C). We manipulated the environmental variables of Environment-L to formulate two additional seasonal environments, i.e. Environment-M (ca. 70°N, Fig. 2D–F) and Environment-H (ca. 80°N, Fig. 2G–I), representing the mid-point and the higher end of the modelled latitudinal gradient (Appendix A). For simplicity, we did not model the sea ice dynamics at any of these higher-latitude environments.

2.2.2. Submodels

2.2.2.1. Growth and development. We used a species-specific formulation to model the growth and development of the copepods, unlike the predecessor model Bandara et al. (2018), which was based on the generic growth formulation of Huntley and Boyd (1984), that tends to

Table 3
Definitions, values and units of the non-evolvable (hard) parameters used in the model. See Table 2 for a description of evolvable (soft) parameters.

Term	Definition	Value/Reference	Units
a	Assimilation coefficient	0.6[4]	–
$A_{i,s,t}$	Mass-dependent ingestion rate (at −2 °C)	Eq. (2)	μg C ind.$^{-1}$ h^{-1}
$A_{i,s,t,z}$	Ingestion rate	Eq. (4)	μg C ind.$^{-1}$ h^{-1}
$A'_{i,s,t,z}$	Temperature-dependent ingestion rate	Eq. (3)	μg C ind.$^{-1}$ h^{-1}
b_s	Mass coefficient of ingestion	Eq. (2), Table 4	–
$B_{i,s,t,z}$	Metabolic rate	Eqs. (14) and (15)	μg C ind.$^{-1}$ h^{-1}
$(B_a)_{i,s,t,z}$	Active metabolic rate	$1.5 \cdot B_b$	μg C ind.$^{-1}$ h^{-1}
$(B_b)_{i,s,t,z}$	Basal metabolic rate	Eqs. (14) and (15)	μg C ind.$^{-1}$ h^{-1}
c_s	Temperature coefficient of ingestion	Eq. (3), Table 4	–
$d_{i,t}$	Parameter for satiation food concentration	0.1–0.3	–
$D_{s,t,z}$	Development time	Eq. (6)	h
$F_{t,z}$	Ambient food concentration	Fig. 2	μg C l^{-1}
f_s	Mass coefficient of metabolism	Table 4	–
$G_{i,s,t,z}$	Growth rate	Eq. (1)	μg C ind.$^{-1}$ h^{-1}
g_s	Temperature coefficient of metabolism	Table 4	–
$H_{i,t,z}$	Survivorship	Eq. (19)	–
i	Individual	–	–
$I_{t,0}$	Irradiance incident on sea surface	Fig. 2	μmol m^{-2} s^{-1}
$I_{t,z}$	Irradiance at depth z	Eq. (9)	μmol m^{-2} s^{-1}
$\acute{I}_{t,z}$	Remapped $I_{t,z}$	0.1–0.9	–
j	Developmental stage	0–12	Egg–Adult
$K_{i,t}$	Scalar for visual predation risk	10^{-6}–10^{-2}	–
$L_{i,t}$	Irradiance sensitivity parameter	1–2.5	–
m_s	Mass exponent of ingestion	Eq. (2), Table 4	–
$(M_n)_{i,t,z}$	Non-visual predation risk	$0.1 \cdot K$	–
$(M_s)_{i,t}$	Starvation risk	Eq. (16)	–
$(M_v)_{i,t,z}$	Visual predation risk	Eq. (10)	–
n_s	Temperature exponent of ingestion	Eq. (3), Table 4	–
N	No. of initial seeds	2.5×10^6	Strategies
o_s	Mass exponent of metabolism	Table 4	–
p_s	Temperature exponent of metabolism	Table 4	–
q_s	Development time parameter-1	Table 4[1, 3]	–
r_s	Development time parameter-2	Table 4[1, 3]	–
$R_{i,s,t,z}$	Fecundity	Eq. (17)	No. of eggs
s	Species	*CF*, *CG*, *CH*	–
$T_{t,z}$	Ambient temperature	Fig. 2	°C
t	Time	1–8760	h
t_R	Time of sexual maturity	1–8760	hour
t_X	Time horizon	1–8760	hour
$U_{i,t}$	Cruising velocity	Eq. (11)	m h^{-1}
W_c	Structural body mass	Fig. 4	μg C
$(W_E)_s$	Species-specific unit egg mass	Table 4	μg C
W_j	Stage-specific critical molting mass	Fig. 4	μg C
$(W_j^{max})_{i,s}$	Stage-specific minimum W_j	Fig. 4	μg C
$(W_j^{min})_{i,s}$	Stage-specific minimum W_j	Fig. 4	μg C
$(W_R)_{i,s,t,z}$	Matter allocated for egg production	Eq. (17)	μg C
W_s	Mass of the energy reserve	–	μg C
$(W_x)_{i,s}$	Catabolized structural mass (proportion of the maximum lifetime structural mass)	0.1–0.5	–
z	Depth	1–1000	m
φ	Termination condition of GA	–	–
ψ	Water column light attenuation coefficient	0.06[2]	m^{-1}
$\Omega_{i,s}$	Fitness	Eq. (18)	–
ω	Weight for fitness	0 or 1[5]	–

[1] Campbell et al. (2001), [2] Eiane and Parisi (2001), [3] Ji et al. (2012), [4] Maps et al. (2012), [5] Bandara et al. (2018).

underestimate growth at lower temperatures (Kimmerer and McKinnon, 1987; Fiksen and Giske, 1995; Bandara et al., 2018). Here, we modelled the somatic growth in carbon (C) units, where the growth rate (G, μg C ind^{-1} h^{-1}) was defined as the balance between assimilation and metabolic rates (Pütter, 1920; Von Bertalanffy, 1938) as,

$$G_{i,s,t,z} = a \cdot A_{i,s,t,z} - B_{i,s,t,z} \tag{1}$$

Here, the assimilation rate is a product of the ingestion rate (A, μg C ind^{-1} h^{-1}) and the assimilation coefficient (a) Huntley and Boyd (1984), where B (μg C ind^{-1} h^{-1}) is the metabolic rate (Section 2.2.2.2.6). Further, i is the individual, s is the species, t is time and z is depth (definitions, units and references of all the terms are listed in Table 3). At a hypothetical reference temperature −2 °C, the ingestion rate relates with the structural mass (W_c, μg C) as,

$$A_{i,s,t} = b_s \cdot (W_c)_{i,t}^{m_s} \tag{2}$$

where b and m are species-specific mass coefficient and exponent of ingestion (Table 4). The ambient temperature (T, °C) elevates the ingestion rate following the exponential function,

$$A'_{i,s,t,z} = A_{i,s,t} \cdot c_s \cdot \exp(n_s \cdot T_{t,z}) \tag{3}$$

where A' is the temperature-dependent (maximum) ingestion rate, and c and n are species-specific temperature coefficient and exponent of ingestion (Table 4). Parameter values for coefficients and exponents of body mass and temperature were estimated following the growth model of Maps et al. (2012) (Table 4, Appendix B). We used an asymptotic function to represent the relationship between the ingestion rate and ambient food concentration (cf. Holling, 1959) as;

$$A_{i,s,t,z} = A'_{i,s,t,z} \cdot \frac{d_{i,t} \cdot F_{t,z}}{1 + d_{i,t} \cdot F_{t,z}} \tag{4}$$

Here, the second product of the right-hand side of the equation scales the temperature-dependent ingestion rate by the ambient food concentration (F, μg C l^{-1}) into a range of 0–1. This posits that on or beyond a satiation food concertation (i.e. the upper asymptote) the growth occurs at a maximum rate dependent only on ambient temperature (Eq. (3)). The parameter d of Eq. (4) (selected range = 0.1–0.3) defines the food concentration at which the asymptotic value of the above relationship is reached (Fig. 3A), and scales with the structural mass (Fig. 3B) as,

$$d_{i,t} = 0.3 \cdot (W_c)_{i,t}^{-0.138} \tag{5}$$

This produces size-specific satiation food concentrations in the range of 75–125 μg C l^{-1} (Fig. 3A), which are comparable to those estimated by Huntley and Boyd (1984), Campbell et al. (2001) and Maps et al. (2012). Despite the variability of nutritional quality of algal food over time and depth largely due to changes in phytoplankton species composition, we used a fixed Chl.-a:C ratio of 0.030 in the above growth estimations for simplicity (Båmstedt et al., 1991; Sakshaug et al., 2009).

Table 4
Species-specific coefficients and exponents of ingestion and respiration (estimated from Maps et al., 2012, Appendix B), along with species-specific egg masses and development time parameters. See Table 3 for term definitions.

Variable	*CF*	*CG*	*CH*
b_s	0.009283	0.01656	0.01319
m_s	0.7524	0.7518	0.7516
c_s	1.2382	1.1606	1.1833
n_s	0.0966	0.0673	0.0761
f_s	0.0008487	0.003292	0.001153
o_s	0.7502	0.7502	0.7502
g_s	1.2956	1.1382	1.2065
p_s	0.1170	0.0585	0.0849
$(W_E)_s$	0.23 μg C[2]	0.40 μg C[3]	0.56 μg C[4]
q_s (eggs)	595[5]	839[6]	1495[6]
q_s (NI)	388[5]	548[6]	974[6]
q_s (NIII)	581[5]	819[6]	1461[6]
r_s (eggs, NI, and NII)	9.11[1]	13.04[1]	13.66[1]

[1] Corkett et al. (1986), [2] Hirche and Bohrer (1987), [3] Hirche (1990), [4] Smith (1990), [5] Campbell et al. (2001), [6] Ji et al. (2012).

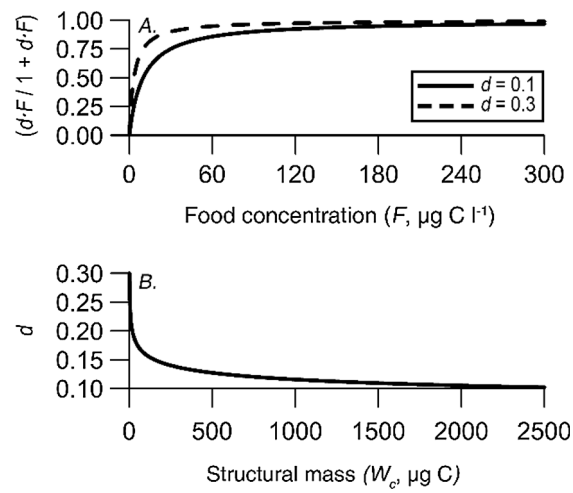

Fig. 3. (A) The shape of the asymptotic function (Eq. (4)) at the higher (0.3) and lower (0.1) ends of parameter d, which describes the dependency of ingestion rate on the ambient food concentration. (B) The power function (Eq. (5)) through which parameter d relates with the structural mass (W_c). In the panel A, the x-intercept of the upper asymptote is ca. 75 μg C l^{-1} for d = 0.3 and 125 μg C l^{-1} for d = 0.1. This is the satiation food concentration, above which ingestion rate becomes solely temperature-dependent (Eq. (3)).

This growth submodel cannot be applied to first and second nauplii stages (NI and NII) which do not feed, but utilize the reserves from the embryo to meet energetic demands (Marshall and Orr, 1972; Mauchline, 1998). Although catabolization of reserves may lead to loss of body mass of non-feeding stages (Maps et al., 2012), for simplicity, we assumed that the structural masses of NI and NII remain constant during development.

The temperature-dependent development times (h) of eggs and non-feeding NI and NII stages were estimated following a Bělehrádek function (Corkett et al., 1986) as,

$$D_{s,t,z} = 24 \cdot [q_s \cdot (T_{t,z} + r_s)^{-2.05}] \tag{6}$$

Here, species-specific values for the parameters q and r were adopted from Campbell et al. (2001) and Ji et al. (2012) (Table 4). While the eggs below the surface mixed layer (Fig. 2) remain stagnant with time, the vertical position of eggs within the mixed layer were determined using a uniformly random probability distribution. The development of feeding stages (NIII–Adult, i.e. from stage j to $j + 1$, where $3 \le j \le 12$) occurs only if the structural mass (W_c) exceeds a stage-specific critical molting mass (W_j, μg C) as,

$$j_{i,s} = \begin{cases} j_{i,s} + 1 & \text{if} \quad (W_c)_{i,s,t} > (W_j)_{i,s} \\ j_{i,s} & \text{if} \quad (W_c)_{i,s,t} \le (W_j)_{i,s} \end{cases} \tag{7}$$

For each model environment, species-specific maximum and minimum estimates of W_j (W_j^{min} and W_j^{max}) were estimated following the growth model of Maps et al. (2012) (Fig. 4, Appendix B). To maintain the intra-specific plasticity of body sizes in the model, we introduced an evolvable parameter α (body size parameter, range = 0–1, Table 2), which defines the stage-specific critical molting masses of any given copepod as,

$$(W_j)_{i,s} = (W_j^{min})_{i,s} + [(W_j^{max})_{i,s} - (W_j^{min})_{i,s}] \cdot \alpha_i \tag{8}$$

Therefore, based on the parameter value of α, the ontogenetic body mass trajectories of copepods tend to occupy a fixed fraction of the

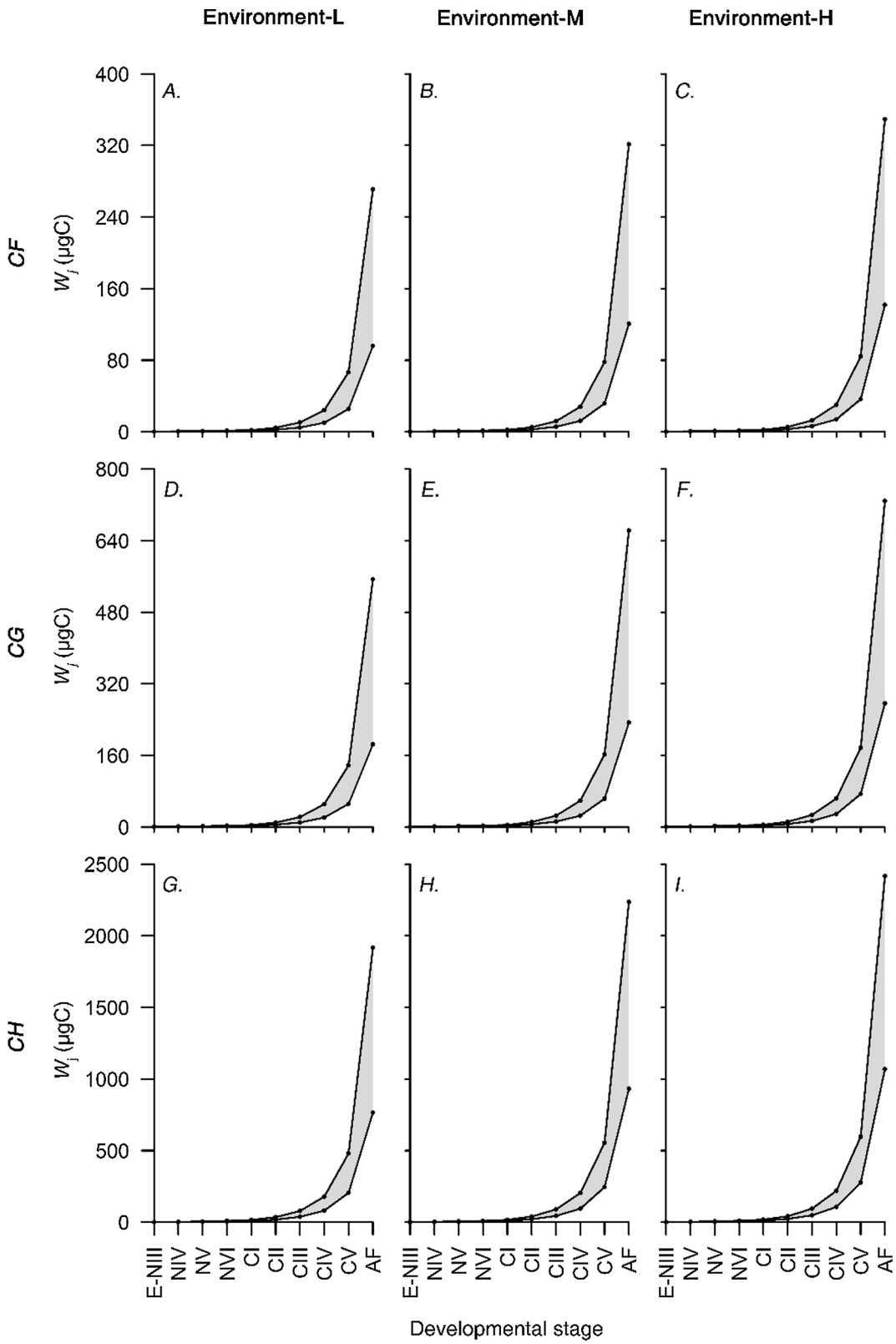

Fig. 4. The species-specific maximum (W_j^{max}: upper line and points in each panel) and minimum (W_j^{min}: lower line and points in each panel) critical molting masses estimated for each model environment. Based on the value of the evolvable body size parameter (α), stage-specific critical molting masses for a given copepod occupies a fixed fraction between the minima and maxima, i.e. within the shaded area (cf. Table B.1 in Appendix B).

environment- and species-specific ranges (Fig. 4, Table B.1 in Appendix B).

2.2.2.2. Survival

2.2.2.2.1. Predation risk. We modelled the predation risk as a probability function. Here, the depth-specific visual predation risk relates with the downwelling irradiance (I) following Eiane and Parisi (2001) as,

$$I_{t,z} = I_{t,0} \cdot \exp(-\psi \cdot z) \tag{9}$$

where I_z and I_0 are irradiance at depth z and surface at a given time, and ψ is the attenuation coefficient for downward directed irradiance in the water column. Although ψ changes over time and depth due to dynamics of phytoplankton biomass and suspended particles in the sea (Lorenzen, 1972; Baker and Lavelle, 1984), we assumed a constant ψ value of 0.06 m^{-1} in this model for simplicity. To express the visual predation risk (M_v) as a probability, we remapped the downwelling irradiance (I) in a range between 0.1 and 0.9 (I') so that visual predation risk offers non-zero probability of survival at the highest possible irradiance level, and non-zero probability of death at the lowest level, expressed as,

$$(M_v)_{i,t,z} = I'_{t,z} \cdot K_{i,t} \tag{10}$$

Here, K is a variable that scales the visual predation risk to produce hourly estimates of mortality.

The detection efficiency of visually orientating planktivores increases with the size of their prey (Brooks and Dodson, 1965; Aksnes and Giske, 1993; De Robertis, 2002; Aljetlawi et al., 2004). Most metrics of detection efficiency, such as predator visual range, reaction distance and electivity index are modelled in a way that it increases rapidly with the initial increase of prey size, while reaching a summit or a plateau as prey size increases further (e.g. Zaret and Kerfoot, 1975; Confer et al., 1978; Pastorok, 1981; Aksnes and Giske, 1993). This is likely due to elevated handling time, prey escape responses and gape-limitations driven by larger prey sizes (Werner, 1974; Fields and Yen, 1997; Devries et al., 1998; Kiørboe, 2011). We followed this logic and modelled the size-dependent visual predation risk as an asymptotic exponential relationship between the body mass (W_c) and K (Fig. 5A), assuming that the largest developmental stage (adult female of *CH*) is ca. 25 times more vulnerable to visual predation risk compared to the smallest developmental stage (egg of *CF*). This scaling accounts for the inclusion of *C. hyperboreus* in this model (*CH*), compared to our previous model of smaller *C. finmarchicus* and *C. glacialis* (Bandara et al., 2018), which used a maximum 10-fold size-dependent visual predation risk scaling.

We modelled the mortality risk imposed by the non-visual predators (M_n) constant over time and depth (Eiane and Parisi, 2001). We chose this representation for its simplicity, while acknowledging the facts that in nature, non-visual predation risk is an entity that varies over space and time, and may play a greater role in shaping-up of behavior and evolution of life histories of high-latitude copepods (e.g. Bandara et al., 2016). In their model, Eiane and Parisi (2001) assumed the non-visual predation risk to account for 0.1% of the maximum visual predation risk. We increased this proportion by an order of magnitude in the predecessor model Bandara et al. (2018), since the 0.1% scale did not have a notable effect on the survivorship of the modelled copepod. In the present model, we assumed that the M_n accounts for 10% of the maximum visual predation risk. This proportional increase of M_n compared to Bandara et al. (2018) accounts for the elevation of the body size of the modelled copepods (Figs. 4 and 5D), that tends to produce more significant hydrodynamic disturbances (during swimming) on which the detection efficiency of most tactile predators rely on (Greene, 1986).

2.2.2.2.2. Diel vertical migration. We used the photoreactive behavior as a proxy to estimate the timing and amplitude of DVM (e.g. Kerfoot, 1970; Carlotti and Wolf, 1998). Here, an evolvable parameter β (irradiance threshold parameter, Table 2) defines an irradiance threshold, above which a negative phototactic response on the vertical swimming behavior is induced (Båtnes et al., 2015; Cohen et al., 2015). Consequently, at any given time, copepods occupy a depth with an irradiance level ($I_{t,z}$) below β. From all possible depth bins that satisfy the $I_{t,z} < \beta$ condition, we assumed that copepods occupy the depth that maximizes the growth potential (Eq. (1)). We predicted this depth deterministically, assuming that copepods are neutrally buoyant and swim vertically in the water column at a constant cruising velocity (U, m h^{-1}) obtained from Bandara et al. (2018) as,

$$U_{i,t} = 8.0116 \cdot (W_c)_{i,t}^{0.4531} \tag{11}$$

For simplicity, we further assumed that internal state-dependent factors, such as hunger and satiation have a negligible influence on the modelled DVM.

To represent the size- or stage-specific variability of DVM (e.g. Zaret and Kerfoot, 1975; Huntley and Brooks, 1982; Hays, 1995; Eiane and Ohman, 2004), we defined an irradiance sensitivity parameter (L, selected range = 1–2.5) that relates positively with structural mass (W_c) following an asymptotic exponential relationship (Fig. 5B). The size-dependent increase of irradiance sensitivity causes the irradiance threshold parameter (β) to decrease as,

$$\beta_{i,t} = \beta_i \cdot \frac{1}{L_{i,t}} \tag{12}$$

The minimum irradiance sensitivity thresholds produced by this model (i.e. 1.4×10^{-7} μ mol m^{-2} s^{-1} for *CF*, 5.92×10^{-8} μ mol m^{-2}

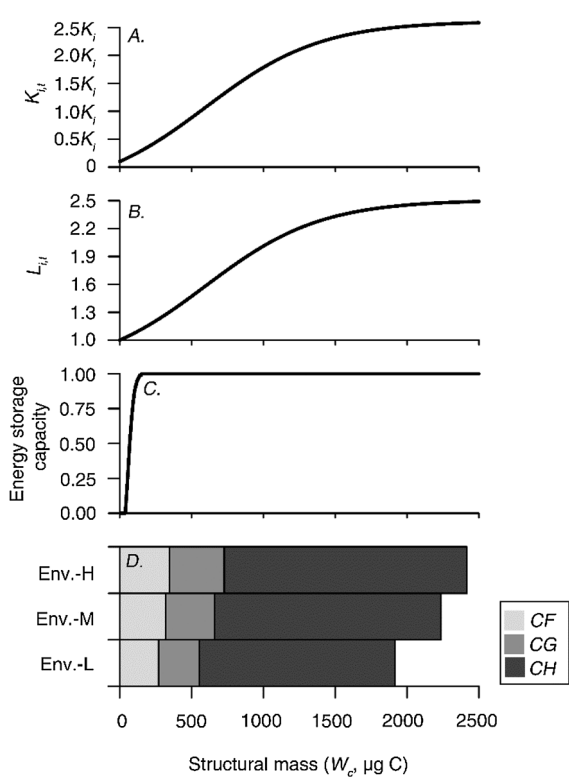

Fig. 5. Size-dependent relationships of (A) visual predation risk scalar K, (B) irradiance sensitivity parameter L, and (C) the energy storage capacity (Eq. (13)). The panel D provide a rough reference to how these size-specific patterns can influence species-specific processes in different model environments.

s^{-1} for *CG* and 3.2×10^{-8} μ mol m^{-2} s^{-1} for *CH*) agree with those published for *Calanus* spp. by Båtnes et al. (2015).

2.2.2.2.3. Energy storage. Developmental stages CIV and CV of *CF* and *CG*, and CIII, CIV and CV of *CH* can allocate an evolvable fraction γ (energy allocation parameter, Table 2) from surplus acquisition to build up an energy reserve. The reserve can occupy up to 70% of the structural mass (Fiksen and Carlotti, 1998; Jónasdóttir, 1999). As a consequence of the body size plasticity allowed in this model, it was observed in the trial runs that copepods always followed the lowest body mass trajectories and overwintered (see below) at a significantly smaller size (W_c ca. 10 μg C for *CF*). This not only disagrees with the body mass estimates of overwintering *Calanus* spp. (Båmstedt et al., 1991; Pepin and Head, 2009), but undermines the concept that a reasonable structural mass should be attained to allow space for the lipid storage (Miller et al., 2000; Lee et al., 2006). Therefore, we defined a minimal structural mass (W_c, μg C) below which no stores can be maintained as,

$$(W_s)_{i,s,t,z} = \begin{cases} 0 & \text{if } (W_c)_{i,t} < 38 \\ G_{i,s,t,z} \cdot \gamma_i \cdot \left[\frac{1}{1 + \exp((60 - (W_c)_{i,t}) / 20)} \right] & \text{if } 38 < (W_c)_{i,t} < 159 \\ G_{i,s,t,z} \cdot \gamma_i & \text{if } (W_c)_{i,t} \geq 159 \end{cases} \tag{13}$$

where W_s (μg C) is the mass of the energy reserve and G is the surplus acquisition (i.e. the growth rate Eq. (1)). Here, energy storage capacity exponentially increases from 38 μg C and approaches an asymptote at 159 μg C (Fig. 5C). These lower and upper W_c values were estimated from lipid sac volume to body size relationships published by Miller et al. (2000) and Vogedes et al. (2010).

2.2.2.2.4. Seasonal vertical migration. We used the state of the energetic reserve as a proxy of timing of the SVM (Visser and Jónasdóttir, 1999). Thus, copepods descend to an overwintering depth when the stores account for an evolvable fraction δ (seasonal descent parameter: Table 2) of the structural mass. For simplicity, we made three general assumptions for selecting overwintering depths. First, copepods always overwinter below the maximum depth of the convective mixed layer (i.e. 500 m) to avoid being circulated back to the surface (Visser and Jónasdóttir, 1999; Irigoien, 2004). Second, the specific overwintering depth below the mixed layer is selected by a gaussian distribution (mean = 750, SD = 50). Third, internal and external environmental variability has no influence on the overwintering depth selection. Although the third assumption does not hold true in nature (e.g. Hirche, 1991; Kaartvedt, 1996; Astthorsson and Gislason, 2003), we used it here for simplicity, because it was shown by Bandara et al. (2018) that the use of an evolvable overwintering depth parameter had little influence on the fitness and phenology of the modelled copepod. After descending to overwintering depths, copepods switch to a diapause state (Carlisle and Pitman, 1961; Hirche, 1996b), where growth, development, vertical movements and reproduction cease (see also Section 2.2.2.2.6). The diapause terminates, and copepods ascend from overwintering depths upon exhausting an evolvable fraction ε from the energy reserve (seasonal ascent parameter, Table 2).

2.2.2.2.5. Generation time. We introduced an evolvable parameter η (generation time parameter, Table 2) to represent the variability of generation times commonly reported for *Calanus* spp. (Table 1). Here, η can take the values of 1, 2 or 3, which indicates the generation time in number of years. However, the present model does not allow generation times < 1 years to be simulated due to a limitation of the fitness function, given the strategy-oriented construct of the model (Section 2.2.3). This tend to constrain the evolutionary plasticity of generation times observed for *C. finmarchicus* at lower latitudes (reviewed in Conover, 1988; Melle et al., 2014). The generation time parameter (η) shows species-specific patterns, where $\eta = 1$ for *CF*, 1 and 2 for *CG* and 1, 2 and 3 for *CH* (cf. Table 1). Generation times > 1 year are characterized by several subsequent seasonal migrations, which follow the same patterns of energy allocation, and same proxies of ascent and descent described above. After the final diapause, copepods do not allocate surplus acquisition to maintain energy reserves.

2.2.2.2.6. Metabolism. The metabolic rate (B, μg C) is the sum of the basal metabolic rate (B_b) and the active metabolic rate (B_a). At the hypothetical reference temperature of −2°C, B_b relates with the total body mass ($W = W_c + W_s$) as,

$$(B_b)_{i,s,t} = f_s \cdot (W)_{i,t}^{o_s} \tag{14}$$

where f and o are mass coefficient and exponent of respiration (Table 4). Ambient temperature elevates B_b following the exponential function,

$$(B_b)_{i,s,t,z} = (B_b)_{i,s,t} \cdot g_s \cdot \exp(p_s \cdot T_{t,z}) \tag{15}$$

where g and p are temperature coefficient and exponent of metabolism (Table 4). Parameter values for above respiration coefficients and exponents were estimated from Maps et al. (2012) (Appendix B). In the model, B_a consists of the swimming cost (i.e. metabolic costs of vertical migrations), which was assumed to be 150% of the B_b (Bandara et al., 2018). During diapause, B_a is nullified (since copepods are assumed stagnant) and the B_b is assumed to reduce by 75% in all species (Maps et al., 2013).

2.2.2.2.7. Starvation. Metabolic demands that cannot be sustained by food intake are balanced by energy reserves. In case of absent or depleted energy reserves, structural mass is catabolized. This induces mortality risk through starvation (starvation risk, M_s). However, we assumed that copepods are tolerant to modest (< 10%) loss of structural mass (Threlkeld, 1976). Structural catabolization beyond this threshold causes the starvation risk to increase linearly and peaks as 50% of structural mass is lost and causes death (Bandara et al., 2018) as,

$$(M_s)_{i,t} = \begin{cases} 0 & \text{if } (W_x)_{i,t} \leq 0.1 \\ 2 \cdot (W_x)_{i,t} & \text{if } 0.1 < (W_x)_{i,t} \leq 0.5 \\ 1 & \text{if } (W_x)_{i,t} \geq 0.5 \end{cases} \tag{16}$$

Here, W_x (μg C) is the catabolized structural mass expressed as a proportion of the maximum structural mass prior to structural catabolization.

2.2.2.3. Reproduction. In this model, somatic growth of copepods ceases after the final molt (e.g. Fiksen and Giske, 1995; Fiksen and Carlotti, 1998; Varpe et al., 2007) and the matter gained through feeding and/or catabolizing energy reserves is allocated for meeting metabolic demands and reproduction. We modelled the energy input to reproduction as a species-specific process. Here, the reproduction of *CF* represents the pure income breeding strategy of *C. finmarchicus* (Table 1), where the energy input is sourced solely from food intake. Reproduction of *CH* represents the pure capital breeding strategy of *C. hyperboreus* (Table 1), where the energy input is sourced entirely from remaining reserves, by allocating a specific amount of carbon

equivalent to the temperature-dependent growth rate (Eqs. (1)–(3)) from the remaining energetic reserve. *CG* represents an intermediate and mixed reproductive strategy similar to that of *C. glacialis* (Table 1), where energy inputs for reproduction may be sourced from both food-intake and energy reserves. The fecundity (R) is estimated using the matter allocated to egg production (W_R, µg C) and the species-specific unit egg mass (W_E, µg C) as,

$$R_{i,s,t,z} = \frac{(W_R)_{i,s,t,z}}{(W_E)_s} \tag{17}$$

Here, W_E varies with the species (Table 4), but we assumed that it is not affected by environmental variability.

2.2.3. Fitness estimation

The performance of behavioral and life history strategies hardwired to each copepod is estimated using a fitness function (Ω, Bandara et al., 2018) that integrates the lifetime survival and reproductive outputs as,

$$\Omega_{i,s} = \left(\sum_{t_B}^{t_X} H_{i,t,z} \cdot R_{i,s,t,z}\right) \cdot \omega \tag{18}$$

Here, ω is a binary weight that adjusts fitness (see below) and H is the survivorship, i.e. the probability of survival from birth (t_B) to a given time horizon (t_X), estimated as a function of visual and non-visual predation risk and starvation risk (M_v, M_n and M_s) as,

$$H_{i,t,z} = \prod_{t_B}^{t_X} 1 - [(M_v)_{i,t,z} + (M_n)_{t,z} + (M_s)_{i,t}] \tag{19}$$

The term ω in Eq. (18) accounts for the persistence of simulated strategies from one generation to the next, assumed that all offspring of a copepod inherit the behavioral and life history strategies (i.e. values of evolvable parameters listed in Table 2) from the parent. This holds true for all other parameters excluding the birth time (t_B), which varies depending on the timing of reproduction of the parent. Consequently, from a series of eggs produced during a copepod's lifespan, only those born in the day of the year similar to the parent can inherit an identical behavioral and life history strategy. Therefore, the value of the binary weight ω is set to 1 if a copepod produces at least one egg with a similar birth time in the following year(s) and vice versa. This fitness weighing process therefore ensures that the modelled behavioral and life history strategies are heritable across generations. Checking for persistence of strategies is necessary because the model does not simulate the life cycles of the offspring (hence the lack of population-level responses) but evaluates fitness of the strategies hardwired to the parents. This characteristic sets the fundamental difference between the present strategy-oriented model and a classic individual-based model. One key limitation of the strategy-oriented construct is that the fitness weighing process knocks-out (i.e. $\omega = 0$ and hence $\Omega = 0$) any strategy that attempts to reproduce within the same calendar year. This prevents life cycles with generation times < 1 year to be simulated in our model.

2.2.4. Operational procedure

2.2.4.1. Initialization

2.2.4.1.1. Seeding. The model operates species- and environment-specifically, i.e. simulations are performed separately for each model species in each model environment. The model initializes with the seeding of N (=2.5 × 10^6) eggs of a selected model species to the near-surface waters (< 50 m) of a selected model environment (Fig. 6). At the time of seeding (=time of birth, t_B), each egg is assigned a predefined behavioral and life history strategy by randomly picking values for the evolvable soft parameters α, β, γ, δ, ε and η (Table 2) from a uniform probability distribution. Five state variables are created to trace the vertical position, structural mass, mass of the energy reserve, survivorship and fecundity of each model copepod (Table 5).

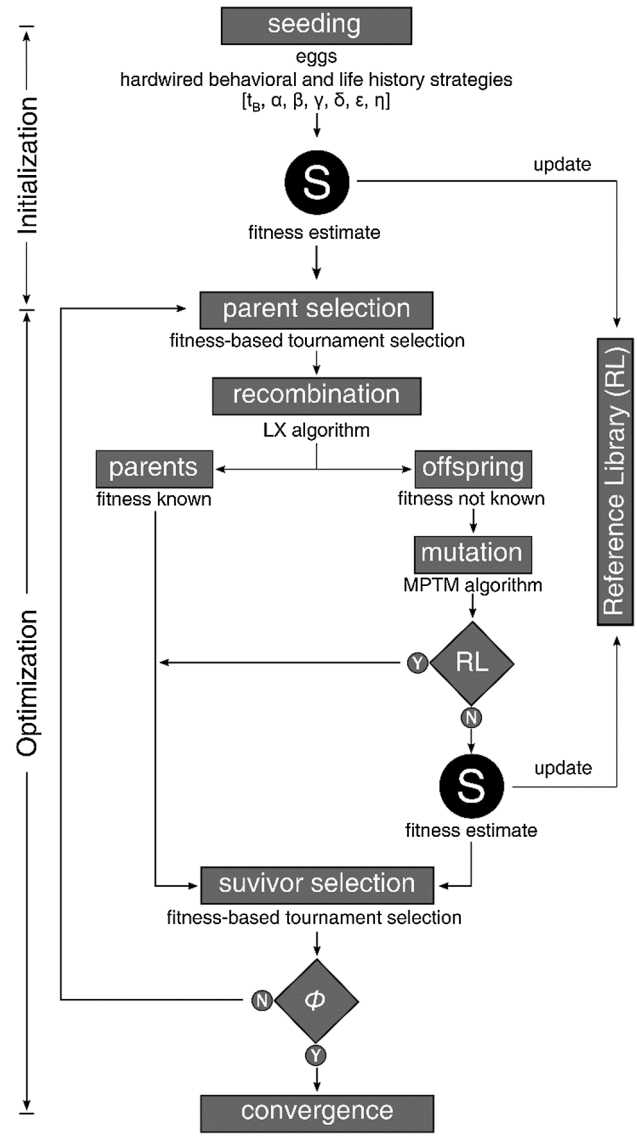

Fig. 6. The two-step operational procedure of the model. At the initialization step, N eggs are seeded and hardwired with randomly generated behavioral and life history strategies. Their life cycles are simulated (symbolized by circled letter S) to produce fitness estimates, which are used in the subsequent GA-driven optimization step. The GA iteratively applies selection, recombination and mutation steps until a termination condition (Φ) is satisfied to heuristically estimate the optimal behavioral and life history strategies that maximize fitness. As a measure of computational efficiency, fitness estimates associated with different strategies are mapped into a reference library (RL), which is updated at each iteration. Y: yes, N: no.

Table 5
Description of the model outputs. Basic outputs are emergent properties of the model, which are logged at each model iteration. Stage-specific outputs are traced at each developmental stage, where state variables are traced throughout the copepod's lifespan at each timestep (=1 h). Stage-specific outputs and state variables are logged only at the final iteration of the model.

Trait/attribute	Units	Description
Basic outputs		
Time of seasonal descent and ascent	Day of the year	Separate estimates representing the timing of SVM, (i.e. the time of descent to overwintering depth and that of the ascent)
Size at seasonal descent	µg C	Structural and energetic reserve mass at the onset of seasonal descent
Overwintering stage	–	Developmental stage at overwintering
Overwintering depth	m	Depth at which the overwintering occurs[a]
Onset of spawning	Day of the year	Time of first egg production
Age of sexual maturity	d	Time since birth to the first egg production
Size at sexual maturity	µg C	Structural mass at first egg production
Total fecundity	No. of eggs	No. of eggs produced during the lifetime
Breeding mode index	–	Proportion of capital breeding eggs (0 = pure income breeding, 1 = pure capital breeding)
Longevity	d	Expected lifespan
Stage-specific outputs		
Surface time	h	Unified estimate representing the timing of DVM, i.e. the stage-specific mean no. of hours per day occupied in waters with highest growth potential (usually the surface waters)
Amplitude of diel vertical migration	m	The vertical range corresponding to the above
Food limitation index	–	Stage-specific total no. hours with food-limited growth as a fraction of stage duration (0 = no food limitation, 1 = total food limitation)
Development time	d	Stage duration, from egg to a given stage
State variables		
Vertical position	m	Depth of occupation at a given time
Structural mass	µg C	Body mass without the energy reserves
Size of the energy reserve	µg C	Mass of the energy reserve
Survivorship	–	Probability of survival at a given time
Fecundity	No. of eggs	No. of eggs produced at a given time

[a] Not an emergent property of the model.

2.2.4.1.2. Initial life cycle simulation. From the time of birth, the model simulates growth and development, survival and reproduction of each model copepod in 1 h timesteps covering the entire lifespan (Fig. 6). The state variables are updated simultaneously. Once the fitness of each copepod is estimated, basic outputs, i.e. the values of the seven evolvable parameters (Table 2), time of seasonal descent and ascent, structural and energy reserve masses at seasonal descent, overwintering stage, age and size at sexual maturity, onset of reproduction, total fecundity, breeding mode index, longevity and fitness are logged/bookkept (see Table 5 for term definitions).

2.2.4.2. Optimization. A Real-Coded Genetic Algorithm (RCGA: Davis, 1989; Lucasius and Kateman, 1989; Herrera et al., 1998) is used to derive environment- and species-specific heuristic estimates of the optimal behavioral and life history strategies that maximize fitness (Fig. 6). In the RCGA, the seven evolvable parameters (Table 2) are considered as genes on a single chromosome. The optimization process begins by selecting a mating pool of N chromosomes (parents) from the initial seeds using a binary (two-way) deterministic tournament (Goldberg and Deb, 1991; Miller and Goldberg, 1995). Genes of two randomly selected parents from the mating pool are recombined following the Laplace crossover method (LX, Deep and Thakur, 2007), which produces two offspring (recombinants). Genes of the recombinants are mutated at a probability of 0.02 per-gene following the Makinen, Periaux and Toivanen method (MPTM, Toivanen et al., 1999).

The population of strategies resulting from the above recombination and mutation operations comprises of N parents, whose fitness are known and N offspring, whose fitness are not yet known (Fig. 6). Parents with unique gene combinations are selected to construct a reference library, which is updated at each iteration. Each offspring is compared with those in the reference library to assess their fitness. The fitness of offspring with similar gene combination to those in the reference library are assigned *in-situ*, while the rest goes through a subsequent life cycle simulation to determine fitness. Once the fitness of all $2N$ individuals are known, N survivors are selected following a round-robin (all-play-all) tournament of size 10 (Harik et al., 1997; Eiben and Smith, 2003). This process is repeated for a minimum of 400 iterations, and terminated when the mean fitness of the population of strategies shows no improvement for a 100 consecutive iterations thenceforth (Eiben and Smith, 2003).

Although the basic outputs are logged during each iteration of the model, the five state variables (Table 5) are not logged until the final iteration. This is to avoid the extensive memory cost of keeping hourly logs of five variables for 2.5×10^6 individuals living up to three years (=26,280 h) for a minimum of 400 iterations. At the final iteration, the model produces an extensive hourly log of the state variables, along with stage-specific logs of surface time, DVM amplitude, food limitation index and stage duration (Table 5).

2.3. Model development, execution and analysis

The model was developed, executed and analyzed using the R™ v.3.3.1 (R Core Team, 2016) and RStudio™ integrated development environment (IDE) v.1.0.136 (RStudio Team, 2016), along with the high-performance computing (HPC) packages Rcpp (Eddelbuettel et al., 2011) and bigmemory (Kane et al., 2013).

A basic run (BR) with default values for model parameters (Table 3) was performed for each model species in the Environment-L. To test the influence environmental variables on the predicted behavioral and life history strategies, we performed a sensitivity analysis following Jørgensen and Bendoricchio (2001), which produces a sensitivity scores (S_x) as,

$$S_x = \frac{(X_{BR} - X_M)/X_{BR}}{(P_{BR} - P_M)/P_{BR}} \tag{20}$$

where X is the predicted model output of the basic run (X_{BR}) and the modified run (X_M) for a given change (± 25%) of input variable value between the basic run (P_{BR}) and the modified run (P_M). Altogether, four different input variables (i.e. food concentration, temperature, non-

visual and visual predation risks) were tested for sensitivity. At each sensitivity run, only the desired input variable value was changed, and all the other variables and parameters of the model were kept unchanged from the BR. Sensitivity analysis was performed separately for each model species.

By performing model runs along the modelled latitudinal gradient at variable levels of visual predation risks we investigated how species-specific behavioral and life history strategies emerge under the influences of bottom-up (i.e. temperature and food availability) and top-down (predation risk) selection pressures (cf. Bandara et al., 2018). Although the food concentration was constant across the model environments, the decreasing duration of the modelled productive season and temperatures ensued a decreasing gradient of growth potential from lower latitude Environment-L to higher latitude Environment-H (Fig. 1, Appendix A). A gradient of visual predation risks was created by varying the scalar K in between 10^{-6}–10^{-2} (i.e. 10^{-6}, 10^{-5}, 10^{-4}, 5×10^{-4}, 10^{-3}, 2.5×10^{-3}, 5×10^{-3}, 7.5×10^{-3} and 10^{-2}). To enhance visualization, we transformed the visual predation risk scalar (K) to its fourth root ($\acute{K}$). In these simulations, the non-visual predation risk was set to 0.1% of the modelled visual predation risk.

As Genetic Algorithms produce heuristic estimates of the maximum fitness, there is no guarantee that it will converge on the global maximum given a potentially diverse fitness landscape (Zanakis and Evans, 1981; Rardin and Uzsoy, 2001; Strand et al., 2002; Record et al., 2010). Therefore, we replicated each model run 10 times with different starting values for the evolvable parameters (Table 2) to check if the algorithm converges on the same set of solutions. As the optimized parameter values showed little variability between replicate runs (< 7%), we used the mean of the replicates for each parameter for analyses.

3. Results and discussion

3.1. Emergent strategies of the basic run

An annual life cycle was predicted for all model species in the basic run (BR). However, the model-predicted optimal behavioral and life history strategy of *CF* was different from the other model species.

The predicted optimal birth times for *CF* occurred in mid-June, when the irradiance and the temperature of the model environment (Environment-L) were at its peak, and the food concentration had decreased by ca. 50% compared to its annual maximum (Fig. 7A). This

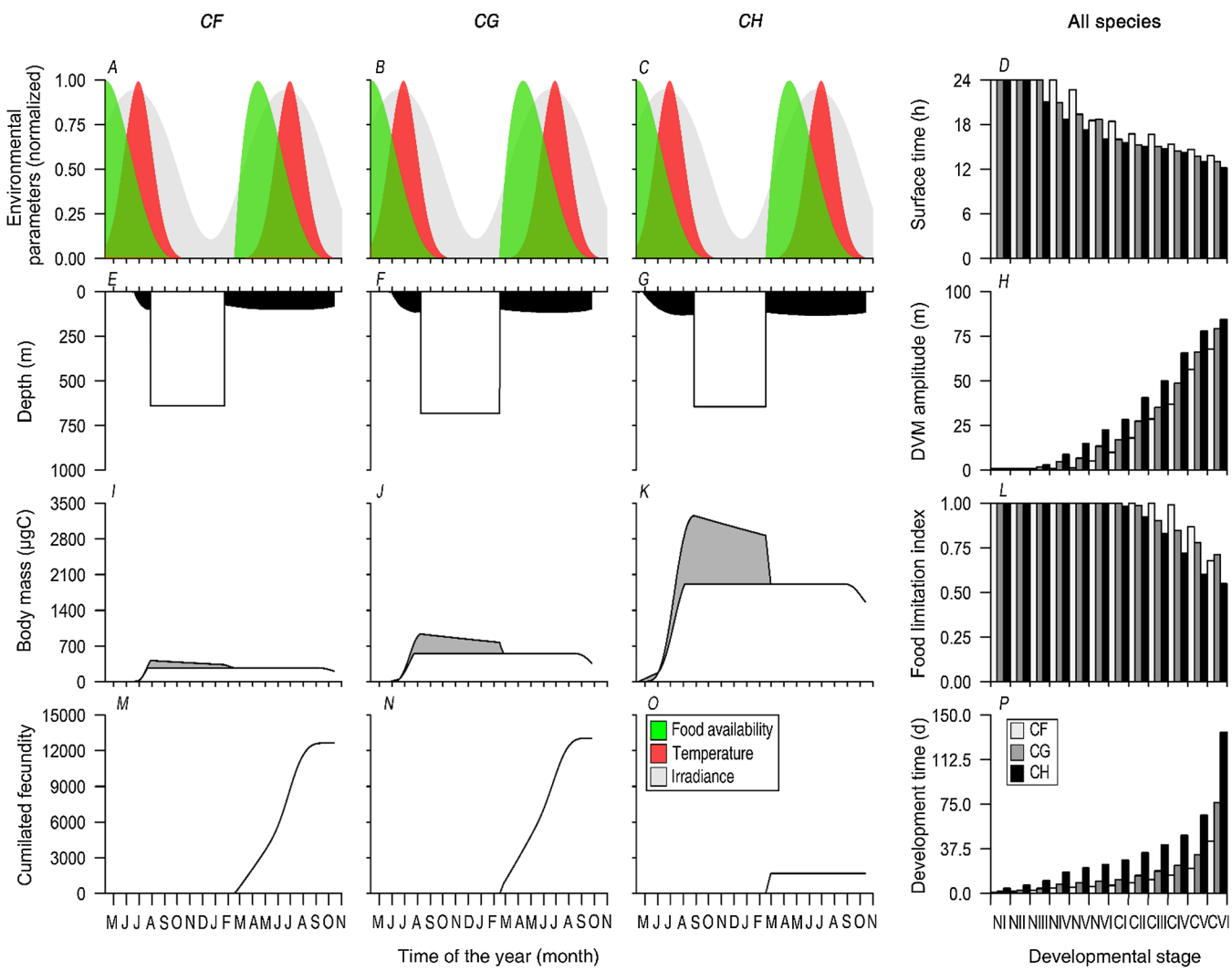

Fig. 7. Some behavioral and life history traits/attributes of the three model species traced in the basic run at Environment-L (A–C, repetitive). To the left are predicted lifetime variability of the vertical trajectories (E–G), structural and energetic reserve masses (I–K) and fecundity (M–O). To the right are stage-specific attributes (D, H, L and P). Shaded regions of panels I–K represent the mass of energy reserve.

seems counterintuitive, as the optimal birth time of *CF* coincided with the annual maximum of visual predation risk (Eqs. (9) and (10)). However, *CF* possessed the smallest body mass among all model species (Fig. 4), and hence was the least vulnerable to visual predation risk (Fig. 5A and D). In addition, due to the smaller size, *CF* became satiated at lower food concentrations (Fig. 3) and suffered least from food-limitation (Fig. 7L). Therefore, it is likely that the smaller body size of *CF* allowed it to utilize higher summertime temperatures to grow and develop faster (Fig. 7P).

The structural growth rate of the late developmental stages of *CF* (CIV onwards) were reduced by two trade-off strategies. First, to minimize the visual predation risk, relatively large developmental stages had to periodically abandon food-rich near-surface waters to perform DVM (down to 50–60 m, Fig. 7D and H). DVM leads to reduced growth and development rates (Houston et al., 1993; Bandara et al., 2018), as growth potential is traded off for survival (Lampert, 1989; Hays, 2003). Second, in order to survive the winter, CIV and CV stages had to allocate a fraction of surplus acquisition to build up energy reserves. The optimal energy allocation parameter (γ, Table 2) predicted for *CF* in the BR was 0.1 (all optimized parameter values are archived in Appendix C and their artificial evolution is demonstrated in Appendix D), which translated to a 10% decrease in structural growth. Consequently, *CF* had to graze toward the end of the productive season to develop in to a pre-adult stage (CV) with sufficient energy reserves to survive the winter (Fig. 7A and E). However, at the time of seasonal descent (late-July: Fig. 7E), *CF* did not carry the maximum possible amount of reserves that it could into diapause (W_s/W_c = 0.54; maximum = 0.70, Fig. 7I). The ascent from overwintering depths occurred in late-January of the following year, before the primary production had commenced, and while the other model species were still in diapause (Fig. 7A, E–G). At the time of seasonal ascent, ca. 43% (59 μg C) of *CF*'s energy reserve remained (seasonal ascent parameter, ε = 0.57: Fig. 7I, Table 2 and Appendix C). However, the CVs emerging from diapause required ca. 14 μg C to reach the size of a sexually mature adult (W_c of overwintering CV ≈ 258 μg C; W_c at sexual maturity ≈ 271 μg C, Fig. 7I). Therefore, it seems that *CF* ascended early from diapause and used the post-overwintering surplus reserves to grow and develop into sexually mature adult females by the onset of pelagic algal bloom. Although this model-predicted seasonal behavior of *CF* somewhat resembles pre-bloom seasonal ascent and spawning patterns observed for *C. finmarchicus* (e.g. Diel and Tande, 1992; Melle and Skjoldal, 1998; Richardson et al., 1999), it doesn't agree with the well-established notion that the seasonal ascent of *C. finmarchicus* occurs after those of *C. glacialis* and *C. hyperboreus* (e.g. Madsen et al., 2001; Astthorsson and Gislason, 2003; Søreide et al., 2008; Bandara et al., 2016). This discrepancy may have emerged due to differential environmental conditions presented in the model compared to their natural habitats. For example, in seasonally ice-covered waters, the earlier seasonal ascent of *C. glacialis* allows it to feed on ice algae and spawn earlier, so that the emergence of first-feeding nauplii (NIII) coincides with the pelagic algal bloom (Søreide et al., 2010). However, the lack of sea ice dynamics and ice-associated primary production doesn't allow this behavior to emerge in our model. Further, field data indicate that the early (late-winter to early-spring) seasonal ascent of *C. hyperboreus* is coupled with a prolonged egg production episode, which continues several months into the productive season (e.g. Plourde et al., 2003). In contrast, the egg production duration of *CH* in the BR of our model often lasted for about one month (possibly due to overestimation of capital allocation rates to egg production), and thus neutralizes any adaptive advantage of an earlier seasonal ascent of *CH* in the BR.

Altogether, the behavioral and life history strategy of *CF* emerging from the BR points to a life strategy that attempts to elevate development rates by allocating more to structural growth at the expense of energy reserves. This strategy is expected from a species which does not use energy reserves for egg production, such as *C. finmarchicus* (Tande et al., 1985; Niehoff et al., 2002; Madsen et al., 2008). It may also be that *CF* in the BR attempted to attain sexual maturity and reproduce within the same productive season. This resembles the life cycle of *C. finmarchicus* in lower latitudes, where it completes several generations per year (e.g. Fish, 1936; Lie, 1965; Matthews et al., 1978; Gislason and Astthorsson, 1996; McLaren et al., 2001; Bagøien et al., 2012). As our model does not allow generation times < 1 year to be simulated, the ability to maintain multiple generations per year and its adaptive significance in the modelled environments remains unclear.

The model-predicted birth times for *CG* and *CH* occurred between mid-April and late-May, ca. 1 month earlier than *CF*. Unlike *CF*, *CG* and *CH* did not employ early birth as a strategy to utilize the seasonal temperature peak to attain higher growth rates. This was likely caused by the increased vulnerability to visual predation risk and the higher satiation food concentrations associated with their relatively large body mass (Figs. 3 and 5A, D). Consequently, *CG* and *CH* were characterized by slower growth rates, pronounced food limitation and 1.5–2 times longer development times compared to *CF* (Fig. 7L and P). Their DVM did not increase much compared to *CF* (Fig. 7D and H) possibly due to occupying a time of the year with lower growth potential, which is in line with observations and predictions of other empirical and modeling work (e.g. Hardy and Gunther, 1935; Huntley and Brooks, 1982; Andersen and Nival, 1991; Fiksen and Giske, 1995; Tarling et al., 2000; Bandara et al., 2018). However, irrespective of the lower growth rates, *CG* and *CH* descended to overwintering depths with maximum possible energy reserves (W_s/W_c = 0.70, Fig. 7J, K). To attain such large reserve loads, older developmental stages (CIII, CIV and CV) allocated up to 40% of the surplus acquisition to reserve build-up, while grazing until the very end of the productive season (Fig. 7F, G).

CG and *CH* adopted a more conservative strategy that prepared themselves for an upcoming overwintering period than striving toward attaining sexual maturity. We interpret this conservative life strategy as a classic adaptation to seasonality in the Arctic pelagic environments (Conover and Siferd, 1993; Hagen and Auel, 2001). The tendency of *CG* and *CH* to elevate energy reserves and overwinter as near-adult size CVs possessed a significant pay-off in the following year, where post-overwintering surplus reserves could solely be allocated to egg production (Fig. 7J, K). *CG* and *CH* ascended in mid-February with the commencement of pelagic primary production (Fig. 7F, G). However, as the food-availability until mid-April (peak bloom) was relatively low, *CG* used the surplus reserves as capital for egg production (Fig. 7B, J, and N). This agrees well with the egg production strategy described for *C. glacialis* (Swift, 1986; Melle and Skjoldal, 1998; Niehoff et al., 2002; Søreide et al., 2010) and is in line with the predictions of life history models for copepods that combine income and capital breeding (e.g. Varpe et al., 2009). The profitability of the mixed income and capital breeding strategy of *CG* was such that its total fecundity was higher compared to the other model species (Fig. 7M–O). The egg production of *CH* ceased ca. 10 d before the peak pelagic bloom, as the reserves were spent on producing nearly 1700 eggs (equivalent to capital input of ca. 950 μg C, Fig. 7K, O). This agrees with the capital breeding strategy described for *C. hyperboreus* (Dawson, 1978; Matthews et al., 1978; Smith, 1990; Hirche, 1997; Scott et al., 2000; Niehoff et al., 2002;

Hirche and Kosobokova, 2003). After spawning, the *CH* females lived toward the end of the productive season without serving any adaptive benefit (Fig. 7G, K, O). This hints at a possibility that if not constrained by our model, these females could have acquired energy reserves and probably spawned again in the following year. Such iteroparous breeding has been commonly suggested for *C. hyperboreus* (Hirche and Kwasniewski, 1997; Swalethorp et al., 2011; Hirche, 2013).

3.2. Sensitivity of emergent strategies to environmental variability

3.2.1. Food concentration

At a 25% higher food concentration ($F = 225\,\mu g\ C\ l^{-1} \approx 7.5$ mg Chl.-*a* m^{-3}), the predicted optimal birth time of *CF* occurred ca. 2 days later compared to BR on June 18 (Fig. 8, Table 6). It seems that *CF* used the higher food concentrations and temperatures later in the year to speed-up structural growth, but allocated less to build up energy reserves, thus entered diapause with 3% less energy reserves compared to BR ($W_s/W_c = 0.52$). Higher food concentration influenced the income breeding egg production of *CF*, which was elevated by ca. 15% compared to the BR.

The influence of elevated food concentration on *CG* and *CH* was notably different from *CF*. The predicted birth times of *CG* and *CH* occurred ca. 2 days earlier (Fig. 8, Table 6), and the growth allocation parameter was ca. 11% higher compared to the BR. Further, ca. 2% increment of structural mass of the overwintering CVs (cf.BR values in Table 6) allowed a little extra space for energy storage at the maximum

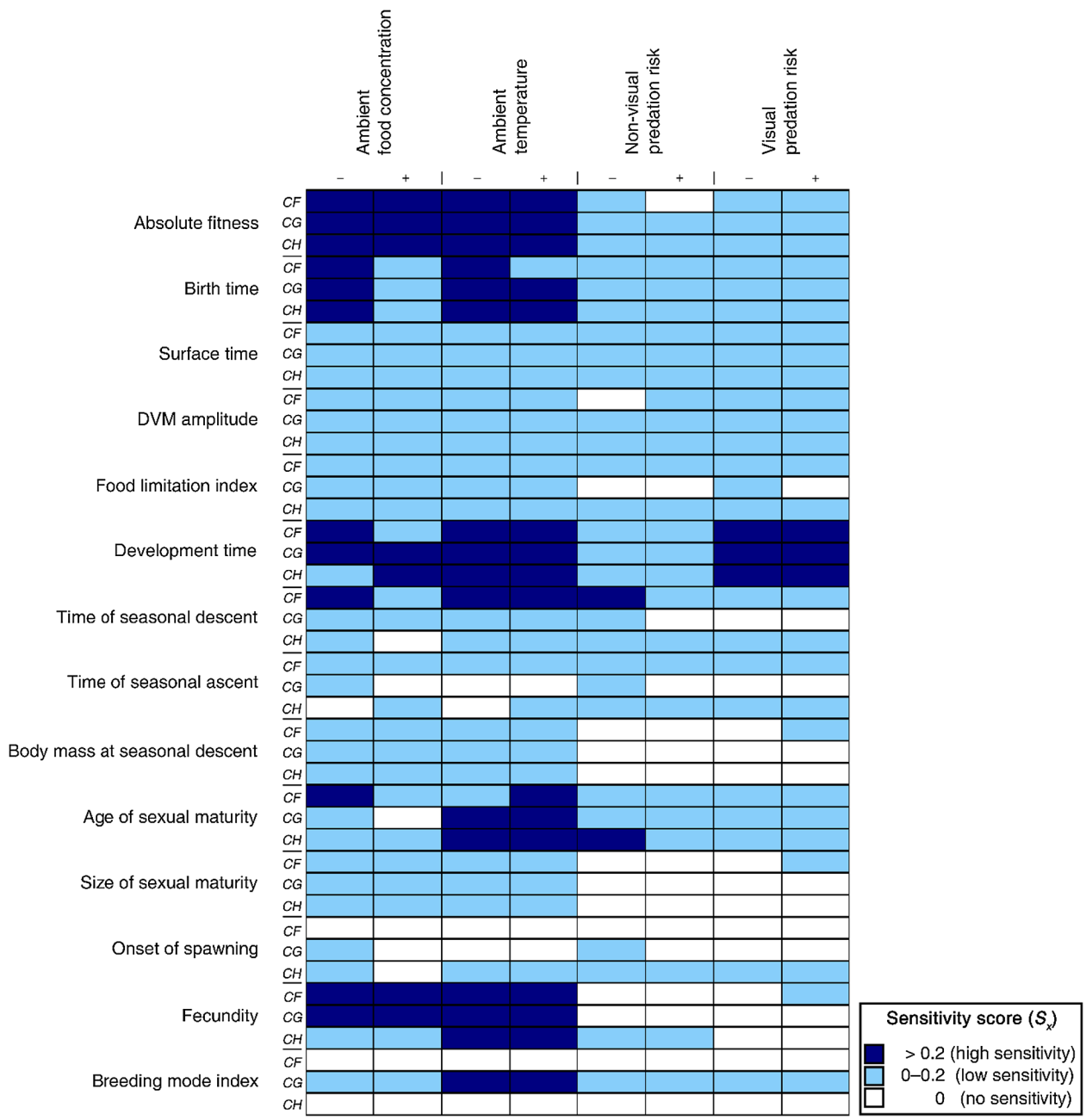

Fig. 8. Graphical summary of the sensitivity analysis. Changes in the variable values (i.e. ± 25% decrease/increase) are on the horizontal dimension, whereas the behavioral and life history traits tested for sensitivity are in the vertical dimension. Further details are provided in Table 6.

Table 6
Influence of ± 25% changes in food concentration (F) and temperature (T) changes on the behavioral and life history strategies emergent from the basic run (BR) for the three model species. Variations of food concentration ranges between $F-$: 135 μg C l^{-1}, $F+$: 225 μg C l^{-1}, and temperature between $T-$: 11.25 °C max and 1.5 °C min, and $T+$: 18.75 °C max and 2.5 °C min. Influences of predation risk are not tabulated due to their lesser significance (cf. Fig. 8).

Species	Scenario tested	Absolute Fitness	Surface time (h)[a]	DVM amplitude (m)[1]	Food-limitation (dim.less)[a]	Development Time (d)[b]	Time of seasonal descent	Time of seasonal ascent	Size at seasonal descent (μg C)	Size at sexual maturity (μg C)	Age at sexual maturity (d)	Onset of spawning (d)	Birth time	Fecundity	Breeding mode index (dim.less)
CF	*BR*	12227.31	19.63	16.12	0.96	44.13	Jul.30	Jan.24	258.31	271.65	244	Feb.16	Jun.16	12,628	0.00
	F+	12870.88	19.40	16.36	0.97	40.19	Jul.28	Jan.29	274.12	276.94	242	Feb.15	Jun.18	13,111	0.00
	F−	11253.92	19.77	16.02	0.94	63.16	Aug.03	Jan.14	249.21	264.43	261	Feb.15	Jun.01	11,621	0.00
	T+	14739.06	19.58	16.09	0.97	32.60	Jul.20	Jan.31	260.55	262.21	242	Feb.15	Jun.18	15,239	0.00
	T−	10337.61	19.56	16.22	0.95	69.75	Aug.13	Jan.14	272.41	283.22	254	Feb.14	Jun.04	10,686	0.00
CG	*BR*	12100.56	18.53	21.87	0.95	76.21	Aug.10	Feb.16	554.38	554.38	266	Feb.16	May.26	13,031	0.07
	F+	12941.16	18.46	21.89	0.97	80.17	Aug.12	Feb.15	563.85	563.85	267	Feb.15	May.24	13,947	0.07
	F−	10838.82	18.82	21.23	0.94	85.08	Aug.05	Feb.16	537.29	537.29	278	Feb.16	May.12	11,649	0.06
	T+	13732.62	18.01	22.47	0.96	59.83	Aug.09	Feb.14	530.66	530.66	248	Feb.14	Jun.11	14,727	0.05
	T−	10797.90	18.67	21.64	0.95	100.91	Aug.07	Feb.14	579.93	579.93	291	Feb.14	Apr.29	11,683	0.08
CH	*BR*	1450.29	18.05	29.51	0.93	135.46	Aug.28	Feb.16	1918.04	1918.04	308	Feb.16	Apr.15	1690	1.00
	F+	1479.60	17.80	30.13	0.95	133.01	Aug.24	Feb.16	1957.79	1957.79	309	Feb.16	Apr.13	1721	1.00
	F−	1376.78	18.19	28.69	0.93	141.62	Aug.21	Feb.16	1860.71	1860.71	319	Feb.16	Apr.02	1609	1.00
	T+	1366.20	17.77	30.12	0.94	96.25	Aug.25	Feb.17	1852.35	1852.35	272	Feb.17	May.21	1583	1.00
	T−	1516.58	18.21	28.92	0.93	152.38	Aug.23	Feb.14	1994.31	1994.31	328	Feb.14	Mar.24	1781	1.00

[a] Mean for all developmental stages.
[b] From egg to adult excluding the overwintering duration.

W_s/W_c ratio of 0.7 (cf. Fig. 5C). Thus, it seems that the higher growth potential led *CG* and *CH* to evolve larger energy reserves rather than larger structural size. Consequently, the number of capital breeding eggs increased for both model species, atop of which, *CG* produced more income breeding eggs, using the higher food concentrations (Table 6).

These findings point to how a small improvement in growth potential caused different evolutionary pathways within the three model species, largely driven by their contrasting breeding modes. Since there was no added advantage of carrying extra energy reserves for the purely income breeding *CF*, it directed the higher growth potential towards accelerating structural growth, which likely reflect a short-term motivation toward attaining sexual maturity within the same calendar year (Roff, 1980; Sainmont et al., 2014; Barta, 2016). However, since the duration of the productive season remained the same as BR (Fig. 2C), SVM and diapause appeared to be inevitable for *CF*. On the other hand, the capital breeding strategy of *CG* and *CH* made them use the elevated growth potential as an investment that increased fecundity in the following year (Table 6, see also Varpe et al., 2009; Ejsmond et al., 2015).

At a 25% lower food concentration (F = 135 μg C l^{-1} ≈ 4.5 mg Chl.-*a* m^{-3}), the differences between the two emergent strategies of the BR appeared to diminish. Here, the predicted optimal birth times of all model species occurred ca. 12–15 d earlier in the year (Fig. 8, Table 6). Due to lowered growth potential (owing to low temperature and food concentration that occur earlier in the year: Fig. 2A–C), they occupied more time in food-rich near-surface waters with reduced DVM and grazed later into the productive season before descending to diapause in late-August. Further, ca. 40% of the surplus acquisition was allocated to building up of energy reserves. Irrespective of the breeding mode, fecundity of all model species decreased by 5–11% (Table 6). Here, the elevated energy reserves of the purely income breeding *CF* indicated a shift towards a more conservative strategy. Storing additional reserves compared to BR reflects the increased difference in the structural masses of the overwintering CV and the adult, which was spanned by allocating the post-overwintering surplus reserves to structural growth in the following year (Table 6). This life history response of *CF* reflects that of *C. finmarchicus* in Arctic locations, which can maintain viable populations in cold and food-limited environments (e.g. Hirche and Kwasniewski, 1997; Madsen et al., 2001; Arnkværn et al., 2005; Hirche and Kosobokova, 2007; Bandara et al., 2016). Conversely, the elevation of energy reserves at lower food concentrations allowed *CG* and *CH* to produce more capital breeding eggs, which is a classic adaptation of some high-latitude zooplankton occupying food-limited seasonal environments (Varpe et al., 2007, 2009).

3.2.2. Temperature

Temperature had the highest influence on the strategies emerging from the BR (Fig. 8). A 25% temperature increase throughout the water column (i.e. T_{max} = 18.75 °C, T_{min} = 2.5 °C) caused a delay in birth times of all model species by 2–35 days (Table 6). This delay became more pronounced in *CG* (16 d) and *CH* (27 d) compared to *CF* (2 d). The delayed birth times of *CG* and *CH* likely allowed them to grow and develop faster in the warmer waters of the late-spring and summer (Fig. 2B). The elevated visual predation risk of inhabiting near-surface waters during the period of seasonal irradiance peak (Fig. 2A) was countered by performing pronounced DVM (Table 6). In all model species, the predicted development times and sizes of the overwintering stages and females decreased (Table 6). Instead of prioritizing structural growth, all model species allocated more of the surplus acquisition to building up of energy reserves and entered diapause with nearly full lipid reserves (W_s/W_c > 0.69). This seems to be driven by the elevated temperature at overwintering depths, which exhausts energy reserves faster than those in the BR (2.5 °C vs 2.0 °C, cf. Eq. (15)). Consequently, the number of capital breeding eggs decreased in *CG* and *CH*. However, due to the elevated assimilation efficiency at higher temperatures (Eq. (3)), income breeding appeared more profitable for *CF* and *CG*, which is

shown by 15–20% increase of fecundity (Table 6). This suggests that in a warmer ocean, *C. finmarchicus* would be more abundant in the high-Arctic (see also, Beaugrand et al., 2002; Chust et al., 2014). Under similar circumstances, the purely capital breeding strategy of *C. hyperboreus* could become disadvantageous, as energy requirements at diapause elevate, and leave less reserves for egg production (Hirche, 1991, 1997; Maps et al., 2013). However, in a warmer ocean, *C. glacialis* will compensate for the loss of fecundity through decreased capital breeding by producing more income breeding eggs (see also Falk-Petersen et al., 2007; Daase et al., 2013, Grote et al., 2015).

At 25% lower temperature throughout the water column (i.e. T_{max} = 11.25 °C, T_{min} = 1.5 °C), all model species were born 2–27 days earlier in the year and occupied more time in near-surface waters with reduced DVM (Table 6). This reflects the longer time needed to develop to diapause stage due to lower growth potential attained in colder waters (Eqs. (1)–(3)). Further, grazing continued toward the very end of the productive season (late August in most cases), and the overwintering CVs of all model species were ca. 2–4% larger than predicted in the BR (Table 6). At the time of seasonal descent, CVs of *CF* had partly filled energy reserves ($W_s/W_c \approx 0.51$). This reflects the decreased diapause metabolic costs at lower temperatures (1.5 °C vs 2.0 °C, cf. Eq. (15)). In contrast, *CG* and *CH* entered diapause with full energy reserves ($W_s/W_c \approx 0.70$) and used the post-overwintering surplus reserves to elevate capital breeding (Table 6). However, only the purely income breeding *CH* had a ca. 10% fecundity gain, while *CF* and *CG* suffered a 12%–15% loss of income breeding potential (and hence the total fecundity, Table 6) due to decreased assimilation efficiency at lower temperatures (Eq. (3)).

3.2.3. Predation risk

Compared to food concentration and temperature, a 25% change in non-visual and visual predation risks had a negligible influence on the emergent behavioral and life history strategies of the BR (Fig. 8). Although low sensitivity of emergent strategies to non-visual predation risk was also predicted by Bandara et al. (2018), the low sensitivity to visual predation risk may be due to that it had operated on a larger range than manifested in the sensitivity analysis (see below).

3.3. Emergent strategies under bottom-up and top-down selection pressures

3.3.1. Emergent strategies at low visual predation risk

At the lowest level of visual predation risk (K' = 0.032), the species-specific behavioral and life history strategies emerging from the model were heavily influenced by the patterns of food availability and temperature. Here, in each model environment, the predicted optimal birth times of all model species occurred earliest in the year (Fig. 9C1–C9). The DVM was less pronounced (Fig. 10A1–A9 and B1–B9), and hence they suffered least from food-limitation (Fig. 10C1–C9). All model species developed relatively slowly due to lower temperatures that occurred earlier in the season (Fig. 2B, E and H), and developed to stage CV with the highest structural and energy reserve masses possible (Fig. 9B1–B9). These large CVs descended to overwintering depths earlier in the year (Fig. 9A1–A9) for diapause. This was followed by an earlier seasonal ascent and reproduction (Fig. 9C1–C9). At the onset of reproduction, females were older compared to higher predation risk levels (Fig. 9D1–D9) and their body masses were the highest (Fig. 9E1–E9). The larger females of *CF* and *CG* could assimilate more efficiently (Eqs. (1) and (2)) and produced the highest number of eggs (Fig. 9F1–F6). The extensive energy reserves of larger overwintering CVs of *CG* and *CH* were used for elevating capital breeding output (Fig. 9F4–F9).

At the lowest level of visual predation risk, environment- and species-specific patterns were also apparent. In *CF*, the birth times shifted ca. 45 days later into the year from mid-April to early-June along the modelled latitudinal gradient (Fig. 9C1–C3). This matched the timing of the peak pelagic bloom in the three model environments (Fig. 2C, F and I). Because of the decreasing gradient of growth potential encountered along the modelled latitudinal gradient and the ca. 20% increase of the size of the overwintering CVs (Fig. 9B1–B3), the timing of seasonal descent shifted by ca. 78 days from late-June to early-September (Fig. 9A1–A3). The timing of seasonal ascent and onset of reproduction also followed an increasing trend along the modelled latitudinal gradient and aligned with the time of the pelagic algal bloom (Figs. 2C, F and I, and 9C1–C3). Because of delayed birth times and elevated development times associated with lower temperatures modelled at higher latitudes (Fig. 2B, E, H), the age of sexual maturity increased along the modelled latitudinal gradient (Fig. 9D1–D3). Further, the size at sexual maturity also increased by ca. 20% (Fig. 9E1–E3). However, the increased size of the female could not compensate for the decreasing assimilation rates induced by lower temperature at higher latitude model environments, as the fecundity decreased by ca. 30% (Fig. 9F1–F3). These findings suggest that *CF* timed its reproduction to match the timing of the pelagic algal bloom along the modelled latitudes. This has been a common observation for *C. finmarchicus*, and reflects the strong dependency of its reproduction on the food availability (Tande and Hopkins, 1981; Aksnes and Magnesen, 1983; Hirche and Kosobokova, 2003; Madsen et al., 2008).

Unlike *CF*, the birth times of *CG* and *CH* did not change much along the modelled latitudinal gradient (Fig. 9C4–C9). At the lower latitude Environment-L, predicted birth times of *CG* and *CH* roughly aligned with the timing of the peak pelagic algal bloom (Figs. 2C, 9C4 and C7). At higher latitude environments, their birth times were predicted ca. 7–25 days ahead of the peak algal bloom (Figs. 2F, I, 9C5, C6, C8 and C9). These temporal offsets roughly align with the cumulative development times estimated from eggs to first feeding NIII stage estimated from Bělehrádek temperature functions (Eq. (6), Table 4), and reflect the descriptions of capital breeding strategies of *C. glacialis* and *C. hyperboreus* in the Arctic, where egg production is timed in a way that first feeding stages can feed under non-limiting food concentrations (e.g. Hirche, 1997; Plourde et al., 2003; Arnkværn et al., 2005; Swalethorp et al., 2011). The pre-bloom egg production of *C. glacialis* is usually observed in seasonally ice-covered coastal habitats, such as shallow seas and fjords (e.g. Kosobokova, 1999; Niehoff et al., 2002; Bandara et al., 2016) and partly fueled by ice-associated primary production (Søreide et al., 2010; Daase et al., 2013). However, despite the lack of ice-associated primary production in our model the emergence of pre-bloom spawning for CG, the *C. glacialis* alias is interesting.

In *CG*, the size of the overwintering CVs increased by ca. 25% along the modelled latitudinal gradient (Fig. 9B4–B6). Given the lower temperatures modelled at higher latitude environments (Fig. 2B, E and H) these larger CVs had to graze toward the end of the productive season to gain sufficient energy reserves for overwintering (Fig. 9A4–A6). The timing of seasonal ascent and reproduction of *CG* showed ca. 60-d delay along the modelled latitudinal gradient (Fig. 9A4–A6 and C4–C6) and reflects the coupling of its reproduction with the timing of the pelagic bloom (Fig. 2C, F and I) despite being a partly a capital breeder

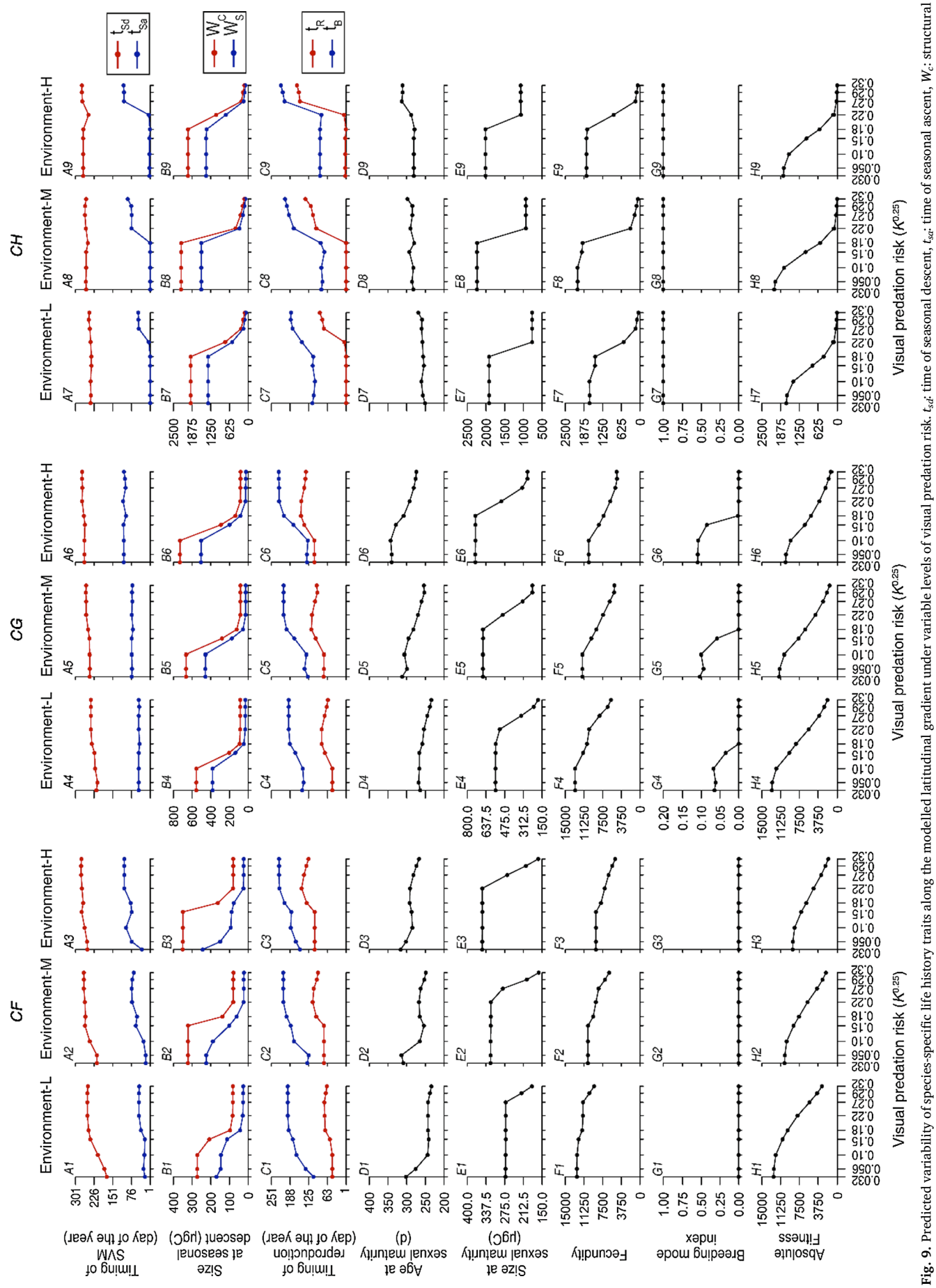

Fig. 9. Predicted variability of species-specific life history traits along the modelled latitudinal gradient under variable levels of visual predation risk. t_{sd}: time of seasonal descent, t_{sa}: time of seasonal ascent, W_c: structural mass, W_s: mass of energy reserve, t_B: optimal birth time, t_R: time of first reproduction.

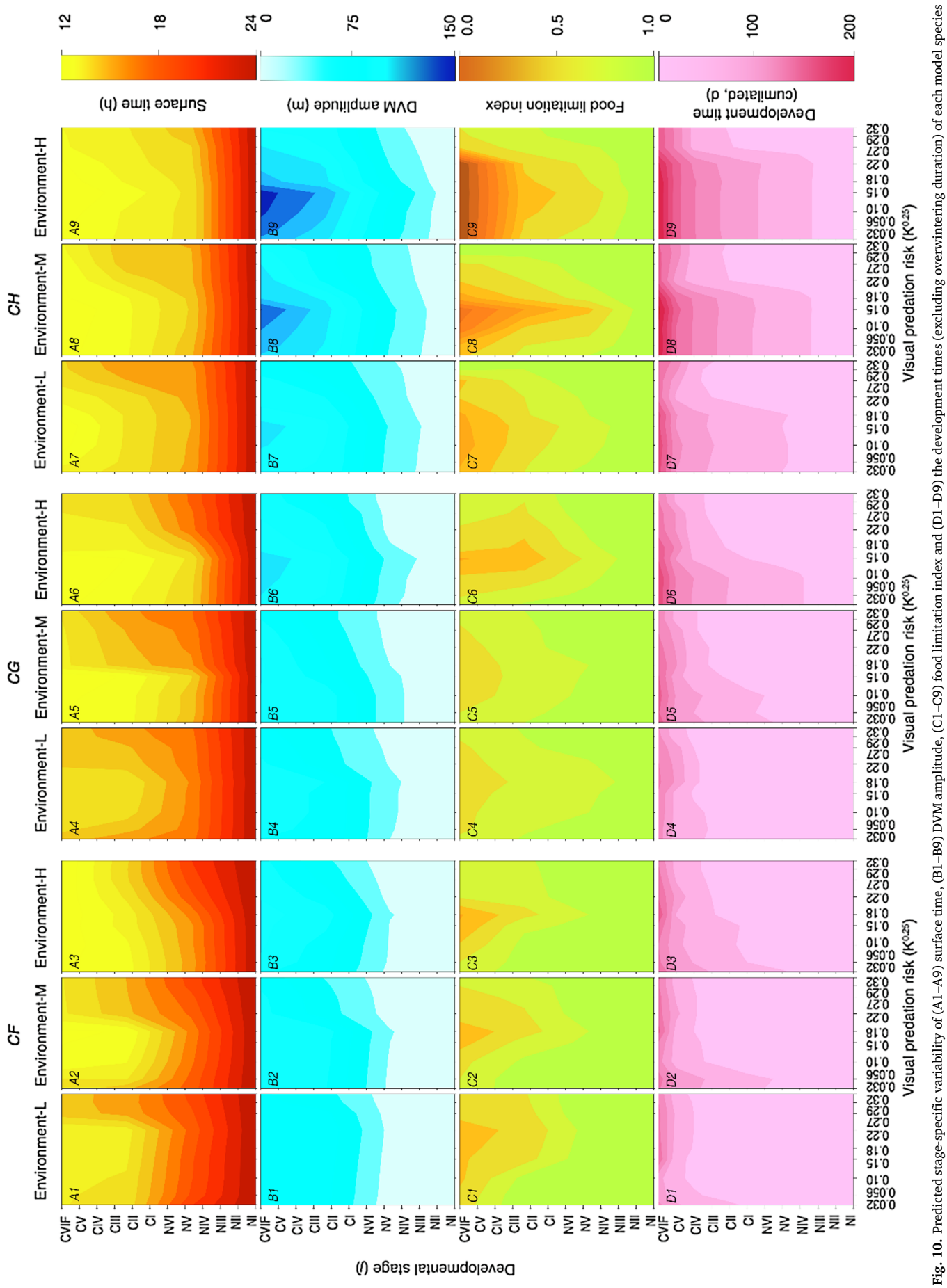

Fig. 10. Predicted stage-specific variability of (A1–A9) surface time, (B1–B9) DVM amplitude, (C1–C9) food limitation index and (D1–D9) the development times (excluding overwintering duration) of each model species along the modelled latitudinal gradient at variable levels of visual predation risk. See Table 5 for descriptions of the above variables.

(Fig. 9G4–G6). Although capital breeding of *CG* accounted for an increasing fraction of the total egg production along the modelled latitudinal gradient (7–11%), the total fecundity decreased by ca. 21% due to the reduced income breeding potential ensued by lower growth potential sustained in higher latitude model environments (Fig. 9F4–F6).

The variability in the timing of SVM and reproduction was least apparent for *CH*. Its timing of seasonal descent showed the least variability along the modelled latitudinal gradient (i.e. ca. 30 days from late-August to late-September, Fig. 9A7–A9), while the timing of seasonal ascent and the onset of reproduction did not change (Fig. 9C7–C9). This reflects the decoupling of *CH*'s reproduction from the timing of pelagic bloom due to its purely capital breeding strategy. The early-January seasonal ascent and the onset of reproduction predicted by our model for the highest latitude model environment (Environment-H) occurs during the Arctic polar night with the pelagic algal bloom several months away (Fig. 2G, I). This aligns with recent field observations on the timing of seasonal ascent and reproduction in several high-Arctic fjords in the Svalbard archipelago between 78° and 80°N (Daase et al., 2014; Błachowiak-Samołyk et al., 2015; Bandara et al., 2016). Given the strict herbivory of the modelled copepods, the viability of these early eggs remains questionable, as NIII emerges within ca. 15 days (at −1.5 °C) after being spawned, which precedes the pelagic bloom by few months and most of these early-born copepods may starve to death. However, lower temperatures at Environment-H (range = −1.5 to 10 °C) tend to extend the reproductive duration of *CH* as the capital allocation rate to egg production in our model is temperature-dependent. Therefore, despite the unviability of early-eggs, those spawned ca. 15–20 d ahead of the pelagic algal bloom would survive. However, in nature, even these early-born copepods may survive, since they can feed on alternative food, such as microzooplankton and ice algae (cf. Runge and Ingram, 1991; Søreide et al., 2008; Campbell et al., 2016).

Although we assumed $K' = 0.032$ as a reference value for extremely low visual predation risk, it had a notable influence on *CH* at the Environment-H. Here, unlike the other model species, *CH* did not follow the maximum potential ontogenetic body mass trajectory (W_j^{max}, cf. Fig. 4I and Table B.1 in Appendix B with the optimized parameter values in Table C.1 in Appendix C). Consequently, the size of the overwintering CV and the size at sexual maturity predicted for *CH* was ca. 11% smaller compared to that predicted for Environment-M (Fig. 9B8, B9, E8 and E9). As the size of the energy reserve was modelled as a fixed (yet, evolvable) fraction of the structural mass, the decreased structural mass translated to a ca. 15% decrease of fecundity (Fig. 9F8 and F9). This finding points to the fact that the adaptive advantage of a larger body size can be highly sensitive to top-down environmental selection pressures (see below).

3.3.2. Emergent strategies at elevated visual predation risk

As the visual predation risk increased from its baseline level of $K' = 0.032$, the bottom-up influences described above diminished, and all model species reacted to visual predation risk in more or less the same manner. The elevated visual predation risk was countered by two strategies; plasticity of behavior and the evolution of body size.

3.3.2.1. Plasticity of behavior: Diel vertical migration. DVM was used to counter relatively modest levels of visual predation risk, i.e. $0.032 \leq K' \leq 0.15$. Here, feeding stages (NII and onwards) of all model species reduced the time spent in warmer, food-rich near-surface waters by descending to depths typically exceeding 100 m (Fig. 10A1–A9 and B1–B9). As reduced surface time decreases feeding opportunities, diel migrants suffered from increased food limitation (Fig. 10C1–C9), which led to reduced growth rates that ultimately elevated development times (Fig. 10D1–D9). To compensate for the DVM-induced loss of growth potential, birth times of all model species shifted later into the year (Fig. 9C1–C9), possibly to utilize higher temperatures that occur later in the season toward attaining higher growth rates (Fig. 2B, E and H). Consequently, they had to feed later into the productive season to fulfil the energy requirements needed to survive the forthcoming unproductive winter and descended to overwintering depths in late-autumn (Fig. 9A1–A9). This late-birth strategy was sufficiently effective that fecundity of all model species remained largely unchanged despite the elevated DVM (Fig. 9F1–F9). An exception to this phenological shift was observed for *CH* at the Environment-H. Here, the timing of birth, SVM, reproduction did not change for the initial increase of visual predation risk despite the predicted larger body size (Fig. 9A9, B9 and C9). At Environment-H, the younger developmental stages (up to NVI) of *CH* did not perform notable DVM (Fig. 9A9, B9). This was caused by the early seasonal ascent and reproduction, which allowed the younger developmental stages to elevate foraging efforts in near-surface waters in a period with lower irradiance and hence lower light-dependent mortality risk (cf. Fig. 2G).

Although DVM is a well-known behavioral response against elevated visual predation risk (reviewed in, Lampert, 1989; Hays, 2003; Brierley, 2014), the influence of DVM on the fitness and phenology of high-latitude copepods has only been highlighted in recent modeling studies (e.g. Bandara et al., 2018). Findings of the above study and those of this investigation agrees well, but do not align with the argument that increased visual predation risk drives earlier seasonal descents (e.g. Kaartvedt, 2000; Varpe and Fiksen, 2010) and diapause (e.g. Ślusarczyk, 1995; Pijanowska and Stolpe, 1996) in marine calanoid copepods and freshwater cladocerans. However, predator population dynamics and the potential for utilization of alternative food sources should be considered toward drawing stronger conclusions.

3.3.2.2. Evolution of body size. As the visual predation risk increased further ($0.15 \leq K' \leq 0.22$), the trading-off of growth potential for survival became unviable. This was caused by the inability to further delay the birth times (Fig. 9C1–C9) in response to elevated DVM, as the growth and development of later developmental stages became constrained by the duration of the productive season. At this point, the model predicted an evolution of body size (i.e. structural and energy reserve masses, W_c and W_s) of overwintering stages. Here, instead of overwintering as larger CV stages with full energy reserves, all species entered diapause as CIV and CIII stages with 50%–90% lower structural and energy reserve masses (Fig. 9B1–B9, see Fig. 4 and Table B.1 in Appendix B for stage-specific critical molting masses). This strategy did not notably reduce the DVM nor the food limitation effects ensued (Fig. 10) but allowed the model species to reduce the predation risk during the ca. 200–350 days long diapause, as in this model, predation risk was not nullified even at greater depths (Eqs. (9) and (10)) (cf. Bandara et al., 2018). The timing of reproduction of all species were significantly delayed by this strategy, as the smaller overwintering stages must use the post-overwintering surplus energy reserves or gains from food intake to elevate their structural mass to attain sexual maturity. This reduced the capital breeding potential of *CG* and *CH*. Further, at $K' \geq 0.18$, *CG* could not produce any capital breeding eggs, and switched its reproductive strategy to pure income breeding (Fig. 9G4–G6).

A further increase of visual predation risk, i.e. $0.22 < K' \leq 0.32$ lead to lower body masses at each developmental stage (NIII onwards). In the model, this was achieved by evolving smaller values for the body size parameter α (Table 2). Modelled copepods with smaller body masses reduced the vulnerability of their younger developmental stages to visual predation, and hence the DVM was restored to the levels observed at lowest level of visual predation risk (Fig. 10A1–A9, B1–B9 and see also Fig. 5A, B). As the copepods could occupy more time on the food-rich near-surface waters, the food limitation of younger developmental stages also decreased (Fig. 10C1–C9). However, birth times did not shift back to occur earlier in the year, probably reflecting the need for the smaller-sized copepods to occupy warmer waters to elevate their assimilation efficiency (see the allometric relationship in Eq. (2)). Consequently, adult females attained sexual maturity at smaller

structural masses, and the expected fecundity decreased dramatically by 20–60% among income breeding *CF* and *CG* (Fig. 9F1–F6). As the capacity to carry energy reserves decreases with body size (Fig. 5C), the capital breeding capacity of *CH* was severely reduced, and its fecundity decreased by ca. 40% at the lower latitude Environment-L, and ca. 96% at the higher latitude Environment-H (Fig. 9F7–F9).

3.4. Concluding remarks

The artificial evolution of body sizes observed in this study resembles the classic field observations of rapid evolution of intra and inter-specific body sizes of zooplankton in response to size-selective predation by planktivorous fish in smaller freshwater lakes (e.g. Brooks and Dodson, 1965; Wells, 1970; Zaret and Kerfoot, 1975). We lack direct observations of this in the Arctic, but such body size responses are predicted from theory (e.g. Stearns et al., 2000) and likely to have contributed to the body size variability across high-latitude *Calanus* species where smaller species are abundant further south (Conover, 1988) where visual and thereby size-selective predation risk is more efficient (Langbehn and Varpe, 2017; Kaartvedt and Titelman, 2018). However, in our model, the body size evolved as the 'last resort', when the increasing visual predation risk could not be countered with behavioral strategies (i.e. DVM). When the visual predation risk elevated beyond the limits of behavioral toleration, it had dramatic consequences on zooplankton life history traits, which appeared to easily outweigh those induced in the bottom-up (Figs. 9 and 10). However, it should be noted that the representation of predation risk in our model is fairly simple, given the elevated computational demands of modelling space and time in superior resolution. Toward an accurate representation of predation risk, biological properties such as, predator morphology, physiology, behavior and population dynamics and physical properties such as, sea-ice dynamics, turbidity, cloud cover and alternative sources of irradiance (e.g. moonlight) should be integrated in to a model (e.g. Aksnes and Giske, 1993; Langbehn and Varpe, 2017).

Elevated visual predation risk obscured the apparent south to north trends in ontogenetic body size patterns (Fig. 9E1–E9, cf. Fig. 4) leading to increased overlap of body size ranges irrespective of the modelled latitude (especially between *CF* and *CG*). Therefore, top-down selection pressures, such as the presence of resident or seasonally migrating populations of planktivorous fish (e.g. Varpe et al., 2005; Renaud et al., 2012) should be considered as an important factor when assessing the potential for misidentifying coexisting *C. finmarchicus* and *C. glacialis* populations using morphometric methods (e.g. Parent et al., 2011; Gabrielsen et al., 2012).

At all scenarios tested, the annual life cycle was the only generation time emerging in this model ($\eta = 1$). Upon further testing we found that > 1-year generation times do emerge when the duration of the pelagic productive season was cut down by ca. 40% under lower levels of visual predation risk ($K' < 0.15$). Therefore, it is likely that the influences of bottom-up selection pressures become more apparent in higher-latitude seasonal environments where resource limitation and year to year environmental variability is more pronounced (Roff, 1980; Fiksen, 2000; Ji, 2011). Unlike the three copepods modelled in our study, whose behavioral and life history strategies evolve in a deterministic environment, the flexibility of generation times is more widespread among all three *Calanus* species (reviewed in Falk-Petersen et al., 2009), especially given the unpredictable environmental conditions encountered in their natural habitats (Broms et al., 2009; Ji et al., 2013a, Hildebrandt et al., 2014). For example, the ability to diapause for several consecutive winters (hence, < 1-year generation time) would be a useful strategy for predominantly herbivorous copepods inhabiting the ice covered waters of the high-Arctic, where timing and duration of the productive season each year is uncertain (Falk-Petersen et al., 2009; Daase et al., 2013).

Due to the difficulty of manipulation of bottom-up and top-down selection pressures in field and laboratory experiments, mechanistic modeling remains as a key tool in the investigation of behavioral shape-up and life history evolution in planktonic animals. However, models are often simple in construct and are based on numerous assumptions, which oftentimes can deviate from the underlying natural phenomena. We tested the reliability of some model assumptions (e.g. prescribed food concentrations, temperature, predation risk levels and fixed model parameters, such as assimilation coefficients) using sensitivity analyses both in the present model and our predecessor model Bandara et al. (2018). However, influences of other model assumptions, such as strict herbivory, light- and size-dependent predation risk formulations and the lack of sea ice dynamics and environmental stochasticity on the model predictions remain to be tested in different modeling approaches. While these limitations provide the motivation to further develop the current model, it also guides the readers through caution while interpreting and extrapolating the present model predictions.

Bottom-up and top-down environmental variability are selection pressures that operates interactively toward shaping-up of behavior and evolution of life histories (Varpe, 2017). Consequently, there are contrasting perspectives about which selective force holds the primacy (Hunter and Price, 1992; Power, 1992; Baum and Worm, 2009). Using a model that allows partitioning the two selection pressures and artificial evolution of seasonal strategies, we argue that top-down selective forces are more significant in the evolution of behavioral and life history strategies of high-latitude copepods.

Acknowledgements

This work was funded partly by VISTA (project no. 6165), a basic research program in collaboration between The Norwegian Academy of Science and Letters and Statoil and the project GLIDER, unmanned ocean vehicles, a flexible and cost-efficient offshore monitoring and data management approach project (No. 269188/E30). ØV received funding from the Fulbright Arctic Initiative and thanks the Woods Hole Oceanographic Institution for hosting during the Fulbright exchange. Authors thank Mark D. Ohman, Espen Strand and Vigdis Tverberg for their valuable suggestions about this work. We are also thankful to the five unanimous reviewers for critically reading the earlier drafts of this manuscript and suggesting substantial improvements.

Appendix A. Summary of environmental variables of the modelled environments

The modeled irradiance was estimated following the global clear-sky horizontal irradiance model of Robledo and Soler (2000). A comprehensive account of the irradiance submodel is provided in Bandara et al. (2018). Estimated irradiance over the modeled environments roughly agree with the field estimates. Field estimates of temperature were adopted from Swift (1986), Ingvaldsen and Loeng (2009), Daase and Eiane (2007), Daase et al. (2013), Bandara (2014), Bandara et al. (2016). Further, temperature and Chlorophyll-a biomass data collected during the UNIS AB820 (2012–2016) cruise from Van Mijenfjorden, Isfjorden, Billefjorden, Kongsfjorden, and offshore stations around 78–81°N were used. Year-round field data (temperature and Chlorophyll-a biomass observations) from Lofoten and Vesterålen regions were also obtained from mooring data via Boris Espinasse (http://love.arctosresearch.net). Finally, temperature data from southern and southeastern Norwegian fjords (60–70°N) were also obtained following communications with Slawek Kwasniweski. These data were considered when deciding the seasonal maxima, minima of temperature and maximum Chlorophyll-a biomass parameterizations.

Table A.1
Comparison between model environments. Cf. Fig. 2 in main text.

Parameter	Attribute	Env-L	Env-M	Env-H
Irradiance (μmol m^{-2} s^{-1})	Min.	0	0	0
	Max.	1500	1200	800
	Time of Max.	day 172 (June 21)	day 172 (June 21)	day 172 (June 21)
Temperature (°C)	Min.	2	0	−1.5
	Max. (°C)	15	12	10
	Time of Max.	day 181 (July 1)	day 203 (July 21)	day 212 (Aug 1)
Food availability (mg m^{-3} Chl.a)	Min.	0	0	0
	Max.	6	6	6
	Time of Max.	day 105 (April 15)	day 135 (May 15)	day 165 (Jun 15)
	Productive season (duration)	229 d	208 d	180 d

Appendix B. The growth and development submodel

Maps et al. (2012) have formulated a mechanistic model to describe growth and development of several high-latitude calanoid copepod species. Their predictions include *Calanus finmarchicus*, *C. glacialis* and *C. hyperboreus*. At constant food concentration and constant temperatures, this growth model performs well. However, in their model, somatic growth (μg C) is estimated as a function of development time.

In the above model, when temperature and food concentration vary over time, the development times tend to shift. For example, a copepod

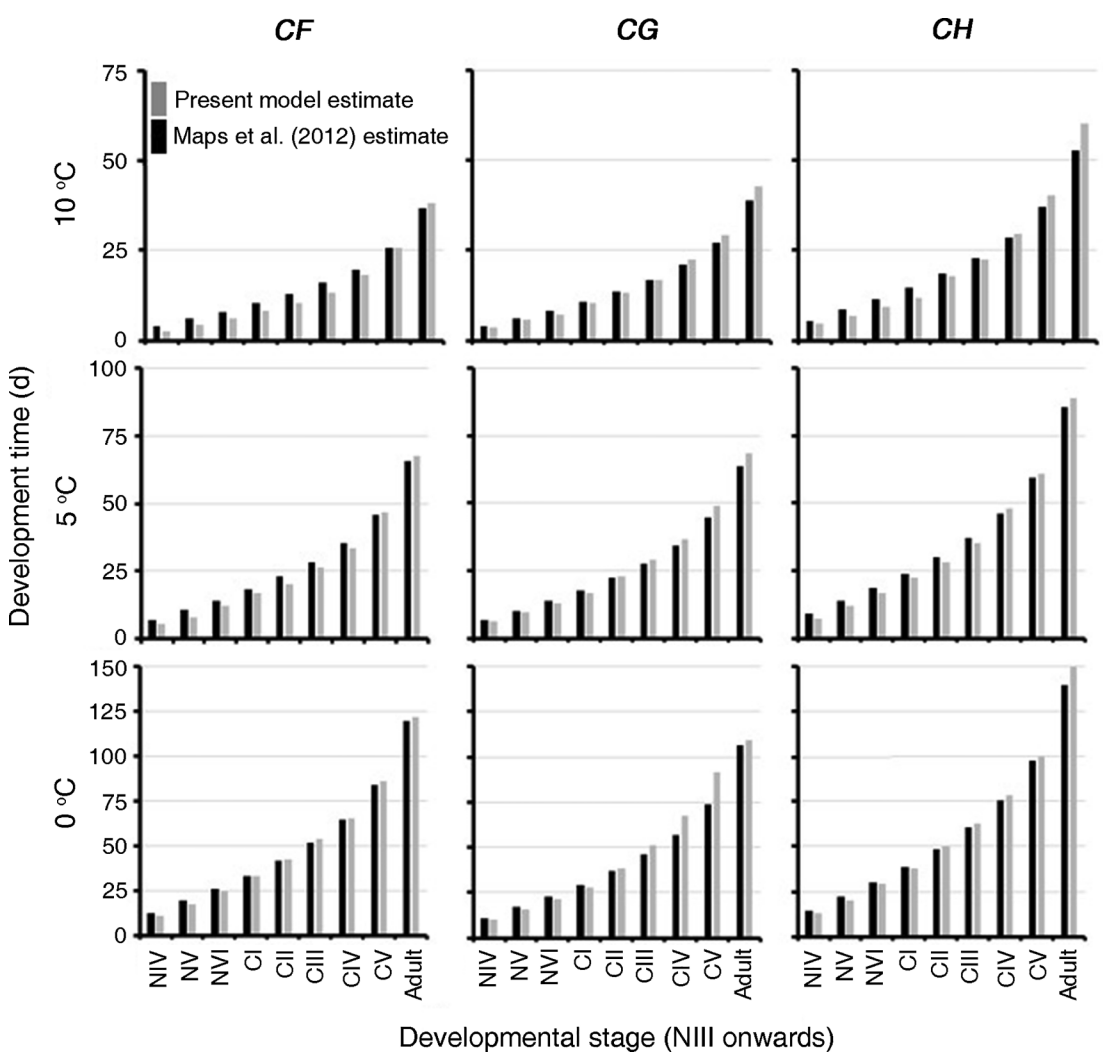

Fig. B.1. Comparison of species-specific development times estimated from Maps et al. (2012) and those of the present study at variable temperatures (10°, 5° and 0 °C) and a constant non-limited food concentration (300 μg C l^{-1}). The stage specific maximum mass reached in the Maps et al. (2012) formulation were used as critical molting masses for the present model. Development time estimates are from egg to a given stage. Data of non-feeding stages are not shown.

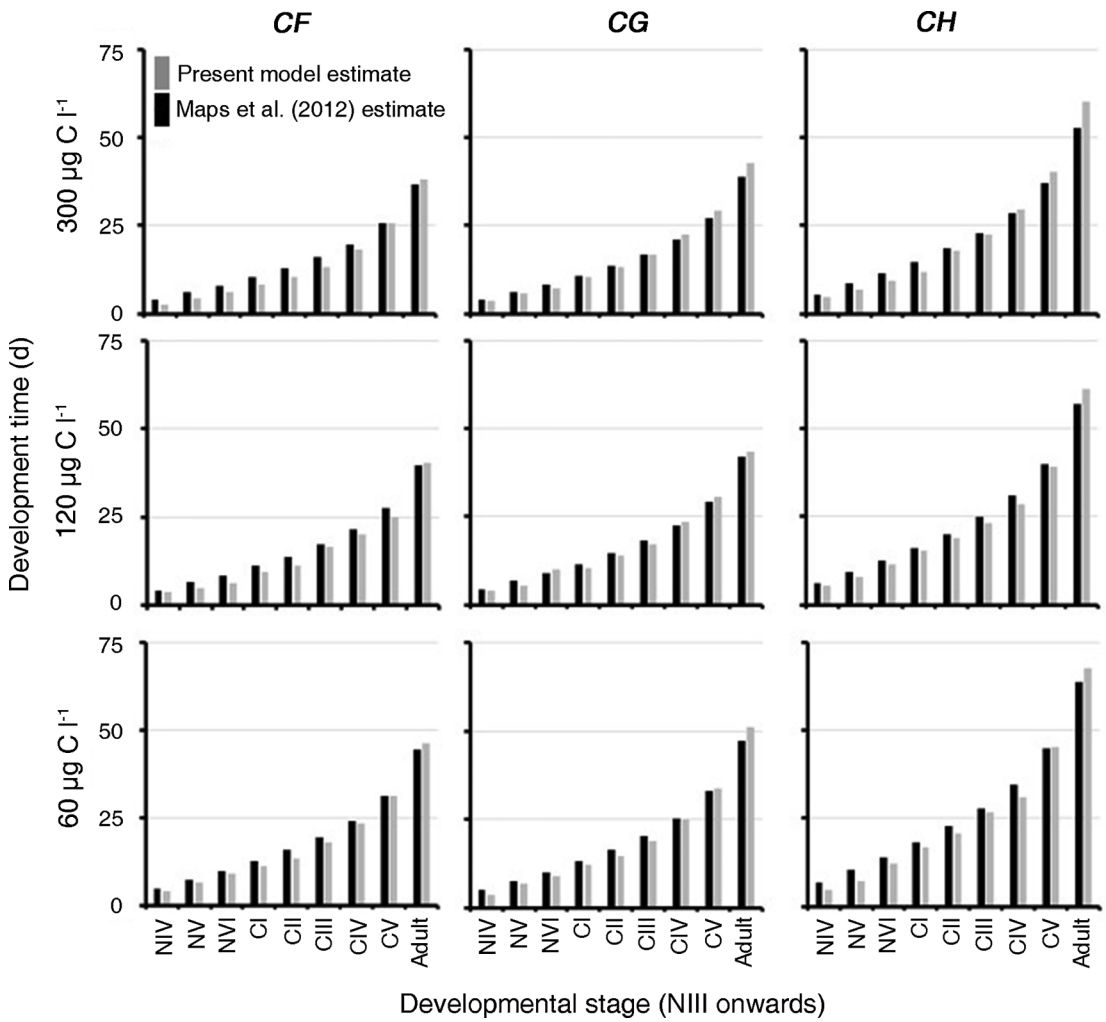

Fig. B.2. Comparison of species-specific development times estimated from Maps et al. (2012) and those of the present study at variable food concentrations (300, 120 and 60 µg C l^{-1}) and a constant temperature (10 °C). The stage specific maximum mass reached in the Maps et al. (2012) formulation were used as critical molting masses for the present model. Development time estimates are from egg to a given stage. Data of non-feeding stages are not shown.

performing DVM would encounter variable temperature and food concentrations on daily if not hourly basis. This variability of development times causes large amounts of Carbon to be assimilated between the development stage j and $j + 1$. We observed that copepods performing DVM attaining unrealistic structural masses as a result (e.g. females with structural masses ca. 4×10^4 µg C at −1 to 10 °C and 0.01–180 µg C l^{-1}). Due to this limitation, we could not implement Maps et al. (2012) growth model as the growth submodel in our work. Another limitation of the above approach is that the development rate becomes undefined at zero food concentration (see their Eqs. (8) and (9)). Although this allows the formulation that *Calanus* spp. are omnivorous, in our study, strict herbivory is assumed. We believe that implementation of omnivory is a next step, especially given that the complicated results such would render, and assumptions involved in modeling of another food source and its seasonality.

However, given the usefulness of the above growth model at constant temperature and food concentrations, we used it to parameterize a simple growth model that we formulated (Eqs. (1)–(8) and (14) and (15)). The temperature and mass coefficients and exponents of our model were estimated from the temperature and mass specific growth predictions (at satiation food concentrations) simulated by Maps et al. (2012)'s model. Predicted development times of the above model and those predicted by ours at constant temperatures and food concentrations agrees fairly well (Figs. B.1 and B.2). Further, at variable temperatures and food concentrations (such experienced by diel migrating copepods) our model produces more meaningful estimates of body size, as development is a function of growth (the concept of critical molting masses, e.g. Fiksen and Giske, 1995; Fiksen and Carlotti, 1998). The only down side to this is that we had to adopt a new evolvable parameter to describe the body mass trajectory.

The critical molting masses (W_j) were calculated from running the Maps et al. (2012) at minimum and maximum environmental specific temperatures (see Table A.1 in Appendix A) under the non-limited food concentration of 180 µg C l^{-1}. Here, the W_j^{max} is given by running the above model at minimum temperature at non-limited food concentration. W_j^{min} was extracted in vice versa scenario (Table B.1).

Table B.1
Minimum (W_j^{min}) and maximum (W_j^{max}) stage-specific critical molting masses (μg C) for each model-species for the three environments. Based on the value of the evolvable body size parameter (α), stage-specific critical molting masses for a given copepod occupies a fixed fraction between the minima and maxima. Estimates were derived following the methods described in Appendix B above. Egg to NIII mass was assumed to remain constant during the development. A graphical representation is provided in Fig. 4 in the main text.

Stage (j)	*CF*						*CG*						*CH*					
	Env.-L		Env.-M		Env.-H		Env.-L		Env.-M		Env.-H		Env.-L		Env.-M		Env.-H	
	W_j^{min}	W_j^{max}	W_j^{min}	W_j^{max}	W_j^{min}	W_j^{max}	W_j^{min}	W_j^{max}	W_j^{min}	W_j^{max}	W_j^{min}	W_j^{max}	W_j^{min}	W_j^{max}	W_j^{min}	W_j^{max}	W_j^{min}	W_j^{max}
E-NIII	0.23	0.23	0.23	0.23	0.23	0.23	0.40	0.40	0.40	0.40	0.40	0.40	0.56	0.56	0.56	0.56	0.56	0.56
NIV	0.44	0.59	0.47	0.62	0.49	0.63	0.90	1.15	0.95	1.21	0.98	1.23	1.94	2.70	2.07	2.86	2.17	2.96
NV	0.61	0.91	0.66	0.97	0.70	1.01	1.31	1.87	1.42	1.98	1.49	2.04	3.36	5.20	3.68	5.63	3.89	5.86
NVI	0.80	1.31	0.89	1.43	0.95	1.49	1.83	2.80	2.01	3.00	2.14	3.11	5.30	8.85	5.89	9.70	6.31	10.17
CI	1.08	1.94	1.23	2.15	1.34	2.26	2.62	4.30	2.92	4.65	3.14	4.87	8.55	15.29	9.62	16.95	10.42	17.90
CII	2.31	4.61	2.66	5.20	2.94	5.51	5.18	9.99	5.97	11.10	6.58	11.77	17.98	35.19	20.72	39.55	22.79	42.09
CIII	4.78	10.49	5.62	12.00	6.35	12.82	10.27	22.37	12.09	25.35	13.66	27.21	37.44	78.37	43.85	88.99	48.54	95.13
CIV	10.18	24.27	12.27	28.10	13.96	30.20	21.11	51.05	25.50	58.91	29.26	63.77	80.48	178.08	95.12	204.15	106.75	219.04
CV	25.68	66.59	31.63	77.94	36.58	84.36	51.54	138.08	63.56	162.21	74.01	177.05	204.98	480.14	244.94	554.96	277.95	597.47
Adult	96.16	271.08	120.91	321.26	141.84	349.34	184.57	553.57	233.59	662.52	276.49	728.69	766.22	1917.90	932.82	2237.50	1068.91	2416.83

Appendix C. Optimized parameters

See Table C.1.

Table C.1
Parameter values optimized in the model. Presented are mean values of the ten replicate runs. The birth time (t_B) is the elapsed no. of hours (= temporal resolution of the model) since 00:00 hrs. of 1st January in a typical 365-day calendar year. Although the generation time parameter (η) can take the values 1, 2 or 3, the model always found the value 1 (= one year generation time) to be optimal.

Run ID	Species ID	Env.	Optimized parameter value (mean of 10 replicate runs)						
			α	β	γ	δ	ε	η	t_B (h)
BR	CF	L	1.00	981	0.10	0.54	0.57	1	3993
	CG	L	1.00	954	0.29	0.70	0.43	1	3481
	CH	L	1.00	902	0.36	0.70	0.29	1	2494
SA F+	CF	L	1.00	970	0.19	0.52	0.49	1	4032
	CG	L	1.00	931	0.41	0.70	0.42	1	2448
	CH	L	1.00	872	0.33	0.70	0.29	1	2821
SA F−	CF	L	1.00	990	0.23	0.63	0.53	1	3660
	CG	L	1.00	969	0.32	0.70	0.44	1	3200
	CH	L	1.00	920	0.30	0.70	0.30	1	2227
SA T+	CF	L	1.00	972	0.10	0.69	0.56	1	4032
	CG	L	1.00	922	0.33	0.70	0.45	1	3904
	CH	L	1.00	861	0.33	0.70	0.31	1	2868
SA T−	CF	L	1.00	973	0.13	0.51	0.47	1	3754
	CG	L	1.00	964	0.23	0.70	0.41	1	2868
	CH	L	1.00	914	0.10	0.70	0.28	1	2014
SA NVPR+	CF	L	1.00	985	0.12	0.54	0.57	1	3918
	CG	L	1.00	952	0.27	0.70	0.43	1	3484
	CH	L	1.00	897	0.36	0.70	0.29	1	2465
SA NVPR−	CF	L	1.00	982	0.15	0.56	0.58	1	4098
	CG	L	1.00	960	0.28	0.70	0.42	1	3489
	CH	L	1.00	909	0.38	0.70	0.29	1	2549
SA VPR+	CF	L	1.00	974	0.13	0.44	0.56	1	4010
	CG	L	1.00	932	0.27	0.70	0.43	1	3581
	CH	L	1.00	890	0.29	0.70	0.29	1	2557
SA VPR−	CF	L	1.00	988	0.16	0.54	0.56	1	3994
	CG	L	1.00	962	0.29	0.70	0.43	1	3415
	CH	L	1.00	912	0.22	0.70	0.29	1	2480
$K' = 0.032$	CF	L	1.00	1000	0.17	0.63	0.60	1	2616
$K' = 0.056$	CF	L	1.00	1000	0.22	0.55	0.65	1	3232
$K' = 0.10$	CF	L	1.00	991	0.10	0.54	0.57	1	3993
$K' = 0.15$	CF	L	1.00	980	0.48	0.55	0.50	1	4277
$K' = 0.18$	CF	L	1.00	924	0.83	0.46	0.73	1	4596
$K' = 0.22$	CF	L	1.00	900	1.00	0.36	0.94	1	4676
$K' = 0.27$	CF	L	1.00	959	1.00	0.34	0.99	1	4687
$K' = 0.29$	CF	L	0.70	974	1.00	0.34	0.99	1	4687
$K' = 0.32$	CF	L	0.50	997	1.00	0.34	1.00	1	4686
$K' = 0.032$	CG	L	1.00	1000	0.19	0.70	0.44	1	3527
$K' = 0.056$	CG	L	1.00	988	0.24	0.70	0.45	1	3420
$K' = 0.10$	CG	L	1.00	935	0.29	0.70	0.43	1	3481
$K' = 0.15$	CG	L	1.00	842	0.55	0.70	0.54	1	4077
$K' = 0.18$	CG	L	1.00	804	1.00	0.55	0.75	1	4522
$K' = 0.22$	CG	L	0.90	891	1.00	0.40	0.99	1	4609
$K' = 0.27$	CG	L	0.40	919	1.00	0.40	0.99	1	4610
$K' = 0.29$	CG	L	0.10	968	1.00	0.40	0.99	1	4610
$K' = 0.32$	CG	L	0.00	972	1.00	0.40	0.99	1	4610
$K' = 0.032$	CH	L	1.00	940	0.26	0.70	0.29	1	2714
$K' = 0.056$	CH	L	1.00	910	0.32	0.70	0.29	1	2592
$K' = 0.10$	CH	L	1.00	876	0.36	0.70	0.29	1	2494
$K' = 0.15$	CH	L	1.00	755	0.27	0.70	0.22	1	2682
$K' = 0.18$	CH	L	1.00	702	0.30	0.70	0.22	1	2628
$K' = 0.22$	CH	L	0.00	714	0.44	0.70	0.28	1	3547
$K' = 0.27$	CH	L	0.00	792	0.54	0.70	0.47	1	4306
$K' = 0.29$	CH	L	0.00	865	0.62	0.70	0.50	1	4448
$K' = 0.32$	CH	L	0.00	919	0.86	0.70	0.56	1	4421

(*continued on next page*)

Table C.1 (*continued*)

Run ID	Species ID	Env.	Optimized parameter value (mean of 10 replicate runs)						
			α	β	γ	δ	ε	η	t_B (h)
$K' = 0.032$	CF	M	1.00	1000	0.10	0.70	0.37	1	3108
$K' = 0.056$	CF	M	1.00	1000	0.26	0.70	0.37	1	2997
$K' = 0.10$	CF	M	1.00	998	0.20	0.59	0.37	1	4176
$K' = 0.15$	CF	M	1.00	984	0.29	0.32	0.64	1	4435
$K' = 0.18$	CF	M	1.00	935	0.55	0.46	0.58	1	4782
$K' = 0.22$	CF	M	1.00	915	1.00	0.31	1.00	1	5032
$K' = 0.27$	CF	M	0.80	944	1.00	0.31	0.99	1	5039
$K' = 0.29$	CF	M	0.40	960	1.00	0.31	0.98	1	5039
$K' = 0.32$	CF	M	0.20	971	1.00	0.29	1.00	1	5049
$K' = 0.032$	CG	M	1.00	1000	0.31	0.70	0.36	1	3069
$K' = 0.056$	CG	M	1.00	1000	0.15	0.70	0.36	1	3346
$K' = 0.10$	CG	M	1.00	994	0.25	0.70	0.36	1	3196
$K' = 0.15$	CG	M	1.00	906	0.48	0.64	0.47	1	4141
$K' = 0.18$	CG	M	1.00	852	0.64	0.49	0.68	1	4779
$K' = 0.22$	CG	M	0.60	864	1.00	0.36	0.97	1	5009
$K' = 0.27$	CG	M	0.20	921	1.00	0.36	0.96	1	5010
$K' = 0.29$	CG	M	0.00	952	1.00	0.36	0.96	1	5011
$K' = 0.32$	CG	M	0.00	996	1.00	0.36	0.96	1	5010
$K' = 0.032$	CH	M	1.00	966	0.16	0.70	0.25	1	1988
$K' = 0.056$	CH	M	1.00	922	0.21	0.70	0.25	1	1907
$K' = 0.10$	CH	M	1.00	894	0.16	0.70	0.25	1	1988
$K' = 0.15$	CH	M	1.00	801	0.29	0.70	0.15	1	1742
$K' = 0.18$	CH	M	1.00	744	0.10	0.70	0.16	1	2040
$K' = 0.22$	CH	M	0.00	732	0.48	0.70	0.37	1	4209
$K' = 0.27$	CH	M	0.00	792	0.54	0.70	0.41	1	4575
$K' = 0.29$	CH	M	0.00	823	0.62	0.70	0.45	1	4751
$K' = 0.32$	CH	M	0.00	939	0.80	0.70	0.53	1	4886
$K' = 0.032$	CF	H	1.00	1000	0.10	0.70	0.29	1	3702
$K' = 0.056$	CF	H	1.00	1000	0.20	0.43	0.52	1	4042
$K' = 0.10$	CF	H	1.00	999	0.24	0.27	0.81	1	4445
$K' = 0.15$	CF	H	1.00	955	0.34	0.40	0.49	1	4383
$K' = 0.18$	CF	H	1.00	921	0.50	0.48	0.54	1	4940
$K' = 0.22$	CF	H	1.00	900	0.99	0.32	0.98	1	5352
$K' = 0.27$	CF	H	0.60	912	1.00	0.31	1.00	1	5365
$K' = 0.29$	CF	H	0.30	939	1.00	0.31	1.00	1	5365
$K' = 0.32$	CF	H	0.10	982	1.00	0.31	1.00	1	5365
$K' = 0.032$	CG	H	1.00	1000	0.19	0.70	0.34	1	3136
$K' = 0.056$	CG	H	1.00	1000	0.19	0.70	0.34	1	3136
$K' = 0.10$	CG	H	1.00	989	0.22	0.70	0.34	1	3079
$K' = 0.15$	CG	H	1.00	921	0.50	0.70	0.43	1	4226
$K' = 0.18$	CG	H	1.00	866	0.66	0.64	0.52	1	4998
$K' = 0.22$	CG	H	0.50	821	1.00	0.38	0.92	1	5365
$K' = 0.27$	CG	H	0.10	940	1.00	0.36	0.95	1	5374
$K' = 0.29$	CG	H	0.00	970	1.00	0.34	1.00	1	5389
$K' = 0.32$	CG	H	0.00	998	1.00	0.34	1.00	1	5390
$K' = 0.032$	CH	H	0.7	1000	0.1	0.7	0.13	1	2089
$K' = 0.056$	CH	H	0.7	940	0.1	0.7	0.13	1	2089
$K' = 0.10$	CH	H	0.7	909	0.1	0.7	0.13	1	2096
$K' = 0.15$	CH	H	0.7	845	0.1	0.7	0.13	1	2093
$K' = 0.18$	CH	H	0.7	788	0.1	0.69	0.13	1	2094
$K' = 0.22$	CH	H	0	720	0.41	0.7	0.19	1	1994
$K' = 0.27$	CH	H	0	770	0.58	0.7	0.43	1	4933
$K' = 0.29$	CH	H	0	913	0.66	0.7	0.45	1	5089
$K' = 0.32$	CH	H	0	946	0.86	0.7	0.49	1	5233

$\boldsymbol{\alpha}$: body size parameter, $\boldsymbol{\beta}$: irradiance threshold parameter, γ: energy allocation parameter, $\boldsymbol{\delta}$: seasonal descent parameter, $\boldsymbol{\varepsilon}$: seasonal ascent parameter, $\boldsymbol{\eta}$: generation time parameter, **BR**: basic run, **SA**: sensitivity analysis, **F** + / −: higher/lower food concentration, **T** + / −: higher/lower temperature, **NVPR** + / −: higher/lower non-visual predation risk, **VPR** + / −: higher/lower visual predation risk, K': forth-root transformed visual predation risk scalar ($K^{0.25}$).

Appendix D. Convergence of parameters and basic output variables in the RCGA in the basic run

See Figs. D.1 and D.2.

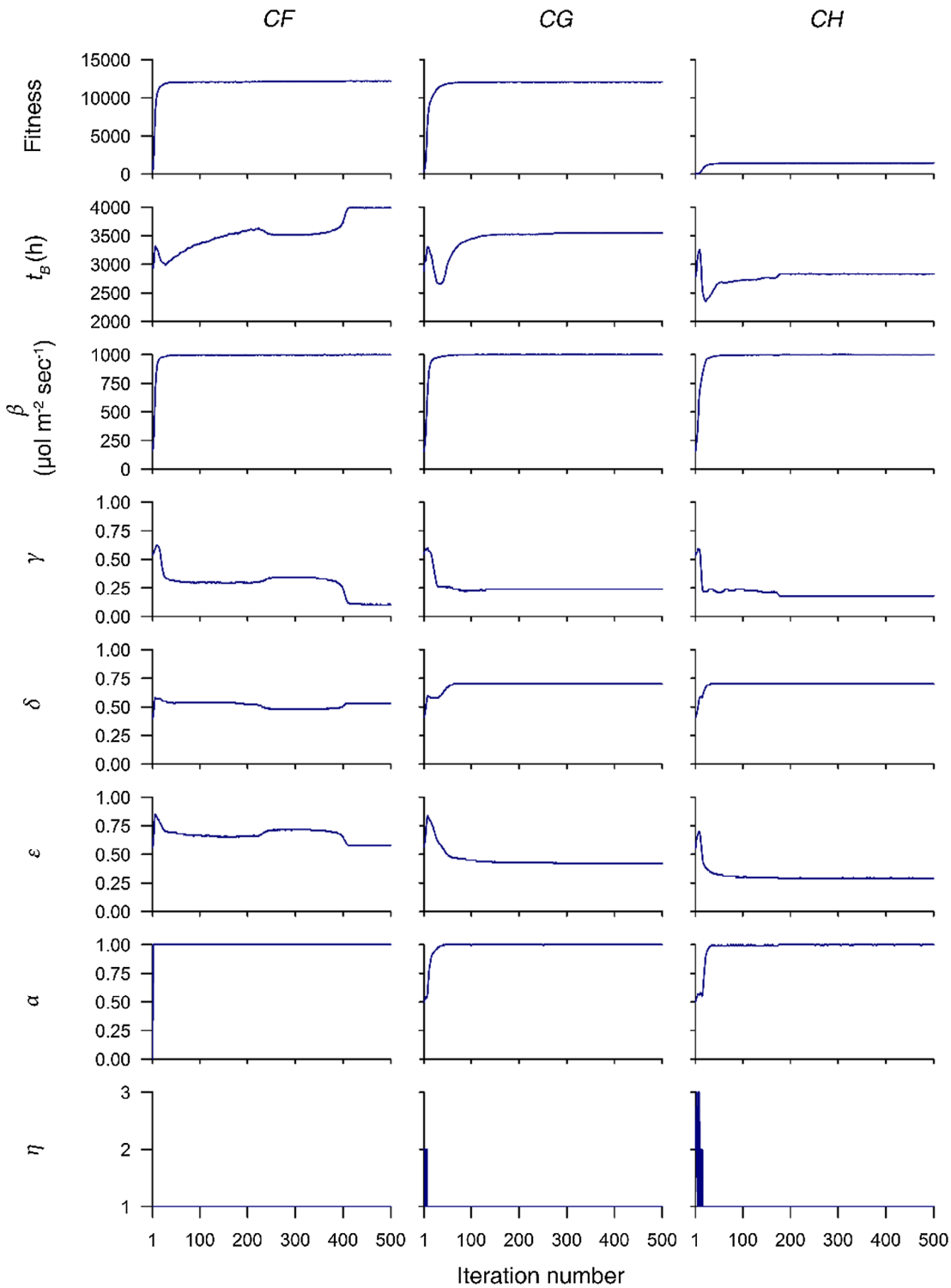

Fig. D.1. Convergence of absolute fitness and the seven evolvable parameters in the optimization process of the basic run. In each iteration, data are presented as the mean of 2×10^6 simulated strategies. In all the modelled species (*CF*, *CG* and *CH*), the optimization process terminated at the generation 500. The birth time (t_B) is the elapsed no. of hours (=temporal resolution of the model) since 00:00 hrs. of 1st January in a typical 365-day calendar year. α: body size parameter, β: irradiance threshold parameter, γ: energy allocation parameter, δ: seasonal descent parameter, ε: seasonal ascent parameter, η: generation time parameter.

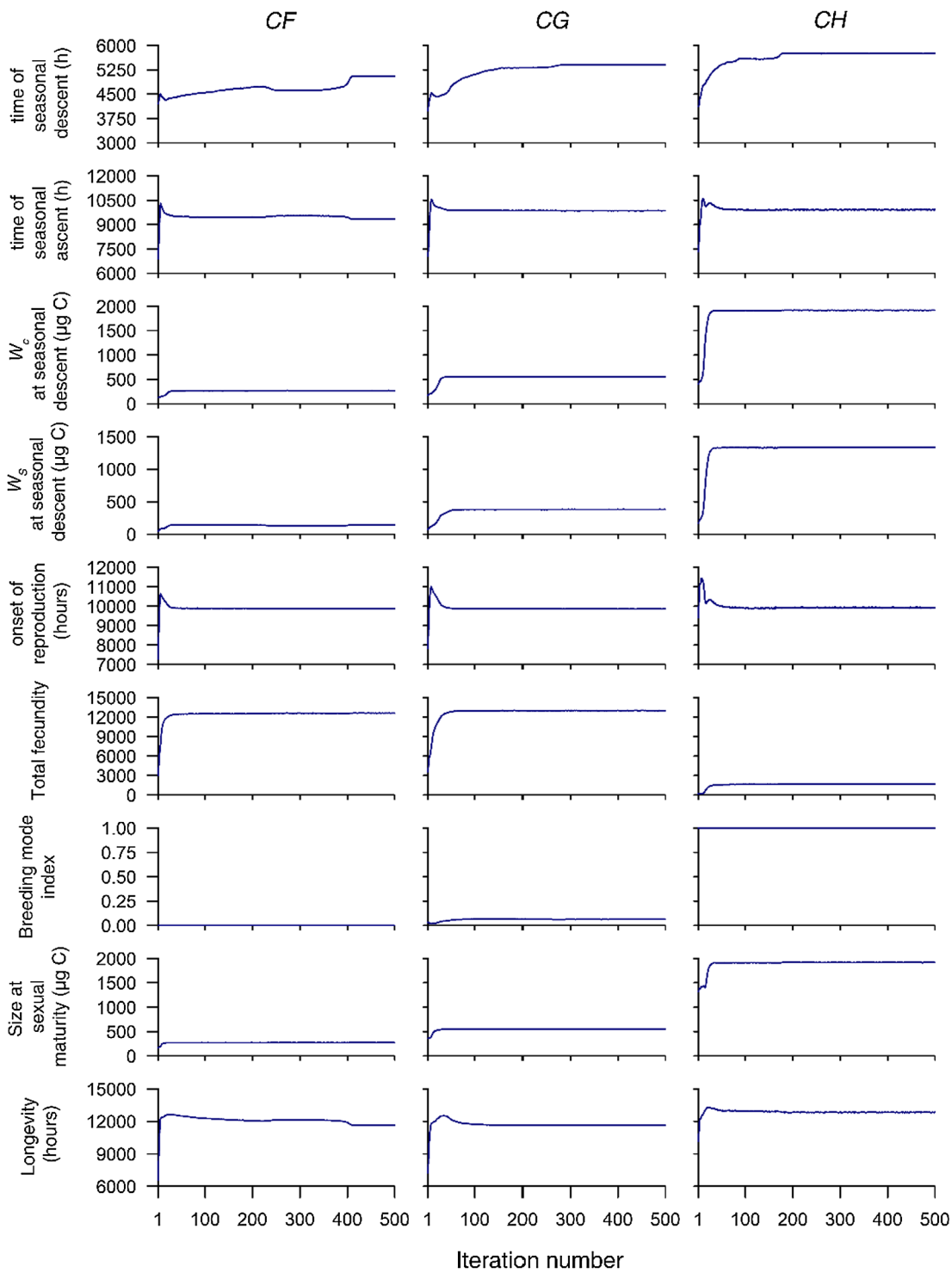

Fig. D.2. Convergence of basic output variables in the optimization process of the basic run. In each iteration, data are presented as the mean of 2×10^6 simulated strategies. In all the modelled species (*CF*, *CG* and *CH*), the optimization process terminated at the generation 500. Times of the year is given in raw format as the elapsed no. of hours (= temporal resolution of the model) since 00:00 hrs. of 1st January in a typical 365-day (= 8760 h) calendar year.

References

Aksnes, D.L., Magnesen, T., 1983. Distribution, development, and production of *Calanus finmarchicus* (Gunnerus) in Lindåspollene, western Norway, 1979. Sarsia 68, 195–207. https://doi.org/10.1080/00364827.1983.10420572.

Aksnes, D.L., Giske, J., 1993. A theoretical model of aquatic visual feeding. Ecol. Model. 67, 233–250. https://doi.org/10.1016/0304-3800(93)90007-F.

Aljetlawi, A.A., Sparrevik, E., Leonardsson, K., 2004. Prey–predator size-dependent functional response: derivation and rescaling to the real world. J. Animal Ecol. 73, 239–252. https://doi.org/10.1111/j.0021-8790.2004.00800.x.

Andersen, V., Nival, P., 1991. A model of the diel vertical migration of zooplankton based on euphausiids. J. Mar. Res. 49, 153–175. https://doi.org/10.1357/002224091784968594.

Arnkværn, G., Daase, M., Eiane, K., 2005. Dynamics of coexisting *Calanus finmarchicus*, *Calanus glacialis* and *Calanus hyperboreus* populations in a high-Arctic fjord. Polar Biol. 28, 528–538. https://doi.org/10.1007/s00300-005-0715-8.

Astthorsson, O.S., Gislason, A., 2003. Seasonal variations in abundance, development and vertical distribution of *Calanus finmarchicus*, *C. hyperboreus* and *C. glacialis* in the East Icelandic Current. J. Plankton Res. 25, 843–854. https://doi.org/10.1093/plankt/25.

7.843.
Bagøien, E., Melle, W., Kaartvedt, S., 2012. Seasonal development of mixed layer depths, nutrients, chlorophyll and *Calanus finmarchicus* in the Norwegian Sea – a basin-scale habitat comparison. Progr. Oceanogr. 103, 58–79. https://doi.org/10.1016/j.pocean.2012.04.014.
Baker, E.T., Lavelle, J.W., 1984. The effect of particle size on the light attenuation coefficient of natural suspensions. J. Geophys. Res.: Oceans 89, 8197–8203. https://doi.org/10.1029/JC089iC05p08197.
Båmstedt, U., Eilertsen, H.C., Tande, K.S., Slagstad, D., Skjoldal, H.R., 1991. Copepod grazing and its potential impact on the phytoplankton development in the Barents Sea. Polar Res. 10, 339–354. https://doi.org/10.3402/polar.v10i2.6751.
Bandara, K., 2014. Mesozooplankton community dynamics in a high arctic fjord. Masters Thesis. Nord University.
Bandara, K., Varpe, Ø., Søreide, J.E., Wallenschus, J., Berge, J., Eiane, K., 2016. Seasonal vertical strategies in a high-Arctic coastal zooplankton community. Mar. Ecol. Progr. Series 555, 49–64. https://doi.org/10.3354/meps11831.
Bandara, K., Varpe, Ø., Ji, R., Eiane, K., 2018. A high-resolution modeling study on diel and seasonal vertical migrations of high-latitude copepods. Ecol. Model. 368, 357–376. https://doi.org/10.1016/j.ecolmodel.2017.12.010.
Barta, Z., 2016. Behavioural change over the annual cycle: optimal annual routines. Curr. Opin. Behav. Sci. 12, 138–141. https://doi.org/10.1016/j.cobeha.2016.11.007.
Båtnes, A.S., Miljeteig, C., Berge, J., Greenacre, M., Johnsen, G.H., 2015. Quantifying the light sensitivity of *Calanus* spp. during the polar night: potential for orchestrated migrations conducted by ambient light from the sun, moon, or aurora borealis? Polar Biol. 38, 51–65. https://doi.org/10.1007/s00300-013-1415-4.
Baum, J.K., Worm, B., 2009. Cascading top-down effects of changing oceanic predator abundances. J. Animal Ecol. 78, 699–714. https://doi.org/10.1111/j.1365-2656.2009.01531.x.
Beaugrand, G., Reid, P.C., Ibanez, F., Lindley, J.A., Edwards, M., 2002. Reorganization of North Atlantic marine copepod biodiversity and climate. Science 296, 1692–1694. https://doi.org/10.1126/science.1071329.
Błachowiak-Samołyk, K., Wiktor, J.M., Hegseth, E.N., Wold, A., Falk-Petersen, S., Kubiszyn, A.M., 2015. Winter Tales: the dark side of planktonic life. Polar Biol. 38, 23–36. https://doi.org/10.1007/s00300-014-1597-4.
Blackburn, T.M., Gaston, K.J., Loder, N., 1999. Geographic gradients in body size: a clarification of Bergmann's rule. Diversity Distrib. 5, 165–174. https://doi.org/10.1046/j.1472-4642.1999.00046.x.
Bollens, S.M., Frost, B.W., 1991. Diel vertical migration in zooplankton: rapid individual response to predators. J. Plankton Res. 13, 1359–1365. https://doi.org/10.1093/plankt/13.6.1359.
Brierley, A.S., 2014. Diel vertical migration. Curr. Biol. 24, R1074–R1076. https://doi.org/10.1016/j.cub.2014.08.054.
Broms, C., Melle, W., Kaartvedt, S., 2009. Oceanic distribution and life cycle of *Calanus* species in the Norwegian Sea and adjacent waters. Deep Sea Res. Part II: Topical Stud. Oceanogr. 56, 1910–1921. https://doi.org/10.1016/j.dsr2.2008.11.005.
Brooks, J.L., Dodson, S.I., 1965. Predation, body size, and composition of plankton. Science 150, 28–35. https://doi.org/10.1126/science.150.3692.28.
Brown, J.H., Gillooly, J.F., Allen, A.P., Savage, V.M., West, G.B., 2004. Toward a metabolic theory of ecology. Ecology 85, 1771–1789. https://doi.org/10.1890/03-9000.
Campbell, R.G., Wagner, M.M., Teegarden, G.J., Boudreau, C.A., Durbin, E.G., 2001. Growth and development rates of the copepod *Calanus finmarchicus* reared in the laboratory. Mar. Ecol. Progr. Series 221, 161–183. https://doi.org/10.3354/meps221161.
Campbell, R.G., Ashjian, C.J., Sherr, E.B., Sherr, B.F., et al., 2016. Mesozooplankton grazing during spring sea-ice conditions in the eastern Bering Sea. Deep Sea Res. Part II: Topical Stud. Oceanogr. 134, 157–172. https://doi.org/10.1016/j.dsr2.2015.11.003.
Carlisle, D.B., Pitman, W.J., 1961. Diapause, neurosecretion and hormones in Copepoda. Nature 190, 827–828. https://doi.org/10.1038/190827b0.
Carlotti, F., Wolf, K.U., 1998. A Lagrangian ensemble model of *Calanus finmarchicus* coupled with a 1D ecosystem model. Fish. Oceanogr. 7, 191–204. https://doi.org/10.1046/j.1365-2419.1998.00085.x.
Chust, G., Castellani, C., Licandro, P., Ibaibarriaga, L., Sagarminaga, Y., Irigoien, X., 2014. Are *Calanus* spp. shifting poleward in the North Atlantic? A habitat modelling approach. ICES J. Mar. Sci. 71, 241–253. https://doi.org/10.1093/icesjms/fst147.
Cohen, J., Berge, J., Moline, M.A., Sørensen, A.J., et al., 2015. Is ambient light during the high Arctic polar night sufficient to act as a visual cue for zooplankton? PloS one 10, e0126247. https://doi.org/10.1371/journal.pone.0126247.
Confer, J.L., Howick, G.L., Corzette, M.H., Kramer, S.L., Fitzgibbon, S., Landesberg, R., 1978. Visual predation by planktivores. Oikos 31, 27–37. https://doi.org/10.2307/3543380.
Conover, D.O., 1992. Seasonality and the scheduling of life history at different latitudes. J. Fish Biol. 41, 161–178. https://doi.org/10.1111/j.1095-8649.1992.tb03876.x.
Conover, R.J., 1965. Notes on the molting cycle, development of sexual characters and sex ratio in *Calanus hyperboreus*. Crustaceana 8, 308–320. https://doi.org/10.1163/156854065X00497.
Conover, R.J., 1967. Reproductive cycle, early development, and fecundity in laboratory populations of the Copepod *Calanus Hyperboreus*. Crustaceana 13, 61–72. https://doi.org/10.1163/156854067X00080.
Conover, R.J., 1988. Comparative life histories in the genera Calanus and Neocalanus in high latitudes of the northern hemisphere. In: Biology of Copepods. Springer, pp. 127–142.
Conover, R.J., Siferd, T.D., 1993. Dark-season survival strategies of coastal zone zooplankton in the Canadian Arctic. Arctic 46, 303–311. https://doi.org/10.14430/arctic1357.
Corkett, C.J., McLaren, I.A., Sevigny, J.M., 1986. The rearing of the marine calanoid copepods *Calanus finmarchicus* (Gunnerus), *C. glacialis* Jaschnov and *C. hyperboreus* Krøyer with comment on the equiproportional rule. Syllogeus 58, 539–546.
Cottier, F.R., Nilsen, F., Skogseth, R., Tverberg, V., Skarðhamar, J., Svendsen, H., 2010. Arctic fjords: a review of the oceanographic environment and dominant physical processes. Geol. Soc., London, Special Publ. 344, 35–50. https://doi.org/10.1144/SP344.4.
Daase, M., Eiane, K., 2007. Mesozooplankton distribution in northern Svalbard waters in relation to hydrography. Polar Biol. 30, 969–981. https://doi.org/10.1007/s00300-007-0255-5.
Daase, M., Falk-Petersen, S., Varpe, Ø., Darnis, G., et al., 2013. Timing of reproductive events in the marine copepod *Calanus glacialis*: a pan-Arctic perspective. Canadian J. Fish. Aquatic Sci. 70, 871–884. https://doi.org/10.1139/cjfas-2012-0401.
Daase, M., Varpe, Ø., Falk-Petersen, S., 2014. Non-consumptive mortality in copepods: occurrence of *Calanus* spp. carcasses in the Arctic Ocean during winter. J. Plankton Res. 36, 129–144. https://doi.org/10.1093/plankt/fbt079.
Davis, L., 1989. Adapting operator probabilities in genetic algorithms. In: Proceedings of the Third International Conference on Genetic Algorithms. Morgan Kaufmann Publishers Inc., George Mason University, USA, pp. 61–69.
Dawson, J.K., 1978. Vertical distribution of *Calanus hyperboreus* in the central Arctic Ocean. Limnol. Oceanogr. 23, 950–957. https://doi.org/10.4319/lo.1978.23.5.0950.
De Robertis, A., 2002. Size-dependent visual predation risk and the timing of vertical migration: an optimization model. Limnol. Oceanogr. 47, 925–933. https://doi.org/10.4319/lo.2002.47.4.0925.
Deep, K., Thakur, M., 2007. A new crossover operator for real coded genetic algorithms. Appl. Math. Comput. 188, 895–911. https://doi.org/10.1016/j.amc.2006.10.047.
Devries, D.R., Stein, R.A., Bremigan, M.T., 1998. Prey selection by larval fishes as influenced by available zooplankton and gape limitation. Trans. Am. Fish. Soc. 127, 1040–1050. https://doi.org/10.1577/1548-8659(1998)127%3C1040:PSBLFA%3E2.0.CO;2.
Diel, S., Tande, K.S., 1992. Does the spawning of *Calanus finmarchicus* in high latitudes follow a reproducible pattern? Mar. Biol. 113, 21–31. https://doi.org/10.1007/BF00367634.
Eddelbuettel, D., François, R., Allaire, J., Chambers, J., Bates, D., Ushey, K., 2011. Rcpp: Seamless R and C++ integration. J. Stat. Software 40, 1–18. https://doi.org/10.18637/jss.v040.i08.
Eiane, K., Parisi, D., 2001. Towards a robust concept for modelling zooplankton migration. Sarsia 86, 465–475. https://doi.org/10.1080/00364827.2001.10420486.
Eiane, K., Ohman, M.D., 2004. Stage-specific mortality of *Calanus finmarchicus*, *Pseudocalanus elongatus* and *Oithona similis* on Fladen Ground, North Sea, during a spring bloom. Mar. Ecol. Progr. Series 268, 183–193. https://doi.org/10.3354/meps268183.
Eiane, K., Tande, K.S., 2009. Meso and Macrozooplankton. In: Sakshaug, E., Johnsen, G.H., Kovacs, K.M. (Eds.), Ecosystem Barents Sea. Tapir Academic Press, Trondheim, Norway, pp. 209–234.
Eiben, A.E., Smith, J.E., 2003. Introduction to Evolutionary Computing, vol. 53 Springer, Berlin, Germany.
Ejsmond, M.J., Varpe, Ø., Czarnoleski, M., Kozłowski, J., 2015. Seasonality in offspring value and trade-offs with growth explain capital breeding. Am. Nat. 186, E111–E125. https://doi.org/10.1086/683119.
Escribano, R., Hidalgo, P., Valdés, V., Frederick, L., 2014. Temperature effects on development and reproduction of copepods in the Humboldt Current: the advantage of rapid growth. J. Plankton Res. 36, 104–116. https://doi.org/10.1093/plankt/fbt095.
Fabian, D., Flatt, T., 2012. Life history evolution. Nat. Educat. Knowledge 3, 10–24.
Falk-Petersen, S., Pedersen, G., Kwasniewski, S., Hegseth, E.N., Hop, H., 1999. Spatial distribution and life-cycle timing of zooplankton in the marginal ice zone of the Barents Sea during the summer melt season in 1995. J. Plankton Res. 21, 1249–1264. https://doi.org/10.1093/plankt/21.7.1249.
Falk-Petersen, S., Pavlov, V., Timofeev, S., Sargent, J.R., 2007. Climate variability and possible effects on arctic food chains: the role of *Calanus*. In: Ørbæk, J.B., KallenbornIngunn, R., Tombre, I., Hegseth, E.N., Falk-Petersen, S., Hoel, A.H. (Eds.), Arctic Alpine Ecosystems and People in a Changing Environment. Springer, Berlin, Germany, pp. 147–166.
Falk-Petersen, S., Mayzaud, P., Kattner, G., Sargent, J.R., 2009. Lipids and life strategy of Arctic *Calanus*. Mar. Biol. Res. 5, 18–39. https://doi.org/10.1080/17451000802512267.
Fields, D.M., Yen, J., 1997. The escape behavior of marine copepods in response to a quantifiable fluid mechanical disturbance. J. Plankton Res. 19, 1289–1304. https://doi.org/10.1093/plankt/19.9.1289.
Fiksen, Ø., Giske, J., 1995. Vertical distribution and population dynamics of copepods by dynamic optimization. ICES J. Mar. Sci. 52, 483–503. https://doi.org/10.1016/1054-3139(95)80062-X.
Fiksen, Ø., Carlotti, F., 1998. A model of optimal life history and diel vertical migration in *Calanus finmarchicus*. Sarsia 83, 129–147. https://doi.org/10.1080/00364827.1998.10413678.
Fiksen, Ø., 2000. The adaptive timing of diapause–a search for evolutionarily robust strategies in *Calanus finmarchicus*. ICES J. Mar. Sci. 57, 1825–1833. https://doi.org/10.1006/jmsc.2000.0976.
Fish, C.J., 1936. The biology of *Calanus finmarchicus* in the Gulf of Maine and Bay of Fundy. Biol. Bull. 70, 118–141. https://doi.org/10.2307/1537318.
Fleminger, A., Hulsemann, K., 1977. Geographical range and taxonomic divergence in North Atlantic *Calanus* (*C. helgolandicus*, *C. finmarchicus* and *C. glacialis*). Mar. Biol. 40, 233–248. https://doi.org/10.1007/BF00390879.
Gabrielsen, T.M., Merkel, B., Søreide, J.E., Johansson-Karlsson, E., et al., 2012. Potential misidentifications of two climate indicator species of the marine arctic ecosystem: *Calanus glacialis* and *C. finmarchicus*. Polar Biol. 35, 1621–1628. https://doi.org/10.1007/s00300-012-1202-7.
Gillooly, J.F., 2000. Effect of body size and temperature on generation time in zooplankton. J. Plankton Res. 22, 241–251. https://doi.org/10.1093/plankt/22.2.241.
Gillooly, J.F., Charnov, E.L., West, G.B., Savage, V.M., Brown, J.H., 2002. Effects of size and temperature on developmental time. Nature 417, 70–73. https://doi.org/10.1038/417070a.
Gislason, A., Astthorsson, O.S., 1996. Seasonal development of *Calanus finmarchicus* along an inshore-offshore gradient southwest of Iceland. Ophelia 44, 71–84. https://doi.org/10.1080/00785326.1995.10429840.

Goldberg, D.E., Deb, K., 1991. A Comparative analysis of selection schemes used in genetic algorithms. In: In: Rawlins, G.J.E. (Ed.), Foundations of Genetic Algorithms, vol. 1. Elsevier, pp. 69–93.
Greene, C.H., 1986. Patterns of prey selection: implications of predator foraging tactics. Am. Nat. 128, 824–839. https://doi.org/10.1086/284608.
Grote, U., Pasternak, A., Arashkevich, E., Halvorsen, E., Nikishina, A., 2015. Thermal response of ingestion and egestion rates in the Arctic copepod *Calanus glacialis* and possible metabolic consequences in a warming ocean. Polar Biol. 38, 1025–1033. https://doi.org/10.1007/s00300-015-1664-5.
Hagen, W., 1999. Reproductive strategies and energetic adaptations of polar zooplankton. Invertebr. Reprod. Develop. 36, 25–34. https://doi.org/10.1080/07924259.1999.9652674.
Hagen, W., Auel, H., 2001. Seasonal adaptations and the role of lipids in oceanic zooplankton. Zoology 104, 313–326. https://doi.org/10.1078/0944-2006-00037.
Hall, D.J., Threlkeld, S.T., Burns, C.W., Crowley, P.H., 1976. The size-efficiency hypothesis and the size structure of zooplankton communities. Annu. Rev. Ecol. System. 7, 177–208.
Hardy, A.C., Gunther, E.R., 1935. The plankton of the South Georgia whaling grounds and adjacent waters, 1926–1927. Discovery Rep. 11, 1–456.
Harik, G.R., Lobo, F.G., Goldberg, D.E., 1997. The compact genetic algorithm. Urbana 51, 61801. https://doi.org/10.1109/4235.797971.
Hays, G.C., 1995. Ontogenetic and seasonal variation in the diel vertical migration of the copepods *Metridia lucens* and *Metridia longa*. Limnol. Oceanogr. 40, 1461–1465. https://doi.org/10.4319/lo.1995.40.8.1461.
Hays, G.C., 2003. A review of the adaptive significance and ecosystem consequences of zooplankton diel vertical migrations. In: In: Jones, M.B., Ingólfsson, A., Ólafsson, E., Helgason, G.V., Gunnarsson, K., Svavarsson, J. (Eds.), Migrations and Dispersal of Marine Organisms Developments in Hydrobiology, vol. 174. Springer, Dordrecht, The Netherlands, pp. 163–170.
Hays, G.C., Richardson, A.J., Robinson, C., 2005. Climate change and marine plankton. Trends Ecol. Evol. 20, 337–344. https://doi.org/10.1016/j.tree.2005.03.004.
Herrera, F., Lozano, M., Verdegay, J.L., 1998. Tackling real-coded genetic algorithms: operators and tools for behavioural analysis. Artificial Intelligence Rev. 12, 265–319. https://doi.org/10.1023/A:1006504901164.
Hildebrandt, N., Niehoff, B., Sartoris, F.J., 2014. Long-term effects of elevated CO_2 and temperature on the Arctic calanoid copepods *Calanus glacialis* and *C. hyperboreus*. Mar. Pollut. Bull. 80, 59–70. https://doi.org/10.1016/j.marpolbul.2014.01.050.
Hirche, H.-J., Bohrer, R.N., 1987. Reproduction of the Arctic copepod *Calanus glacialis* in Fram Strait. Mar. Biol. 94, 11–17. https://doi.org/10.1007/BF00392894.
Hirche, H.-J., 1990. Egg production of *Calanus finmarchicus* at low temperature. Mar. Biol. 106, 53–58. https://doi.org/10.1007/BF02114674.
Hirche, H.-J., 1991. Distribution of dominant calanoid copepod species in the Greenland Sea during late fall. Polar Biol. 11, 351–362. https://doi.org/10.1007/BF00239687.
Hirche, H.-J., Hagen, W., Mumm, N., Richter, C., 1994. The Northeast Water Polynya, Greenland Sea: III. Meso- and macrozooplankton distribution and production of dominant herbivorous copepods during spring. Polar Biol. 14, 491–503. https://doi.org/10.1007/BF00239054.
Hirche, H.-J., 1996a. Diapause in the marine copepod, *Calanus finmarchicus*—a review. Ophelia 44, 129–143. https://doi.org/10.1080/00785326.1995.10429843.
Hirche, H.-J., 1996b. The reproductive biology of the marine copepod, *Calanus finmarchicus*—a review. Ophelia 44, 111–128. https://doi.org/10.1080/00785326.1995.10429842.
Hirche, H.-J., Niehoff, B., 1996. Reproduction of the Arctic copepod *Calanus hyperboreus* in the Greenland Sea-field and laboratory observations. Polar Biol. 16, 209–219. https://doi.org/10.1007/BF02329209.
Hirche, H.-J., 1997. Life cycle of the copepod *Calanus hyperboreus* in the Greenland Sea. Mar. Biol. 128, 607–618. https://doi.org/10.1007/s002270050127.
Hirche, H.-J., Kwasniewski, S., 1997. Distribution, reproduction and development of *Calanus* species in the Northeast Water in relation to environmental conditions. J. Mar. Syst. 10, 299–317. https://doi.org/10.1016/S0924-7963(96)00057-7.
Hirche, H.-J., Kosobokova, K.N., 2003. Early reproduction and development of dominant calanoid copepods in the sea ice zone of the Barents Sea—need for a change of paradigms? Mar. Biol. 143, 769–781. https://doi.org/10.1007/s00227-003-1122-8.
Hirche, H.-J., Kosobokova, K.N., 2007. Distribution of *Calanus finmarchicus* in the northern North Atlantic and Arctic Ocean—expatriation and potential colonization. Deep Sea Res. Part II: Topical Stud. Oceanogr. 54, 2729–2747. https://doi.org/10.1016/j.dsr2.2007.08.006.
Hirche, H.-J., Kosobokova, K.N., 2011. Winter studies on zooplankton in Arctic seas: the Storfjord (Svalbard) and adjacent ice-covered Barents Sea. Mar. Biol. 158, 2359. https://doi.org/10.1007/s00227-011-1740-5.
Hirche, H.-J., 2013. Long-term experiments on lifespan, reproductive activity and timing of reproduction in the Arctic copepod *Calanus hyperboreus*. Mar. Biol. 160, 2469–2481. https://doi.org/10.1007/s00227-013-2242-4.
Holland, J.H., 1975. Adaptation in Natural and Artificial Systems. An Introductory Analysis with Application to Biology, Control, and Artificial Intelligence, vol. 1 University of Michigan Press, Ann Arbor, Michigan, USA.
Holling, C.S., 1959. Some characteristics of simple types of predation and parasitism. Canadian Entomol. 91, 385–398. https://doi.org/10.4039/Ent91385-7.
Hopkins, C.C.E., Tande, K.S., Grønvik, S., Sargent, J.R., 1984. Ecological investigations of the zooplankton community of balsfjorden, Northern Norway: an analysis of growth and overwintering tactics in relation to niche and environment in *Metridia longa* (Lubbock), *Calanus finmarchicus* (Gunnerus), *Thysanoessa inermis* (Krøyer) and *T. raschi* (M. Sars). J. Exp. Mar. Biol. Ecol. 82, 77–99. https://doi.org/10.1016/0022-0981(84)90140-0.
Houston, A.I., McNamara, J.M., John, M.C.H., 1993. General results concerning the trade-off between gaining energy and avoiding predation. Philos. Trans.: Biol. Sci. 341, 375–397. https://doi.org/10.1016/0022-0981(84)90140-0.
Hunter, M.D., Price, P.W., 1992. Playing chutes and ladders: heterogeneity and the relative roles of bottom-up and top-down forces in natural communities. Ecology 73, 724–732. https://doi.org/10.2307/1940152.
Huntley, M.E., Brooks, E.R., 1982. Effects of age and food availability on diel vertical migration of *Calanus pacificus*. Mar. Biol. 71, 23–31. https://doi.org/10.1007/BF00396989.
Huntley, M.E., Boyd, C., 1984. Food-limited growth of marine zooplankton. Am. Nat. 124, 455–478. https://doi.org/10.1086/284288.
Huntley, M.E., Lopez, M.D.G., 1992. Temperature-dependent production of marine copepods: a global synthesis. Am. Nat. 140, 201–242. https://doi.org/10.1086/285410.
Irigoien, X., 2004. Some ideas about the role of lipids in the life cycle of *Calanus finmarchicus*. J. Plankton Res. 26, 259–263. https://doi.org/10.1093/plankt/fbh030.
Ingvaldsen, R., Loeng, H., 2009. Physical oceanography. In: Sakshaug, E., Johnsen, G.H., Kovacs, K. (Eds.), Ecosystem Barents Sea. Tapir Academic Press, Trondheim, Norway, pp. 33–64.
Jaschnov, W.A., 1972. On the systematic status of *Calanus glacialis*, *Calanus finmarchicus* and *Calanus helgolandicus*. Crustaceana 22, 279–284. https://doi.org/10.1163/156854072X00561.
Jeppesen, E., Jensen, J.P., Søndergaard, M., Fenger-Grøn, M., et al., 2004. Impact of fish predation on cladoceran body weight distribution and zooplankton grazing in lakes during winter. Freshwater Biol. 49, 432–447. https://doi.org/10.1111/j.1365-2427.2004.01199.x.
Ji, R., 2011. *Calanus finmarchicus* diapause initiation: new view from traditional life history-based model. Mar. Ecol. Progr. Series 440, 105–114. https://doi.org/10.3354/meps09342.
Ji, R., Ashjian, C.J., Campbell, R.G., Chen, C., et al., 2012. Life history and biogeography of *Calanus* copepods in the Arctic Ocean: an individual-based modeling study. Progr. Oceanogr. 96, 40–56. https://doi.org/10.1016/j.pocean.2011.10.001.
Ji, R., Jin, M., Varpe, Ø., 2013a. Sea ice phenology and timing of primary production pulses in the Arctic Ocean. Global Change Biol. 19, 734–741. https://doi.org/10.1111/gcb.12074.
Ji, R., Stegert, C., Davis, C.S., 2013b. Sensitivity of copepod populations to bottom-up and top-down forcing: a modeling study in the Gulf of Maine region. J. Plankton Res. 35, 66–79. https://doi.org/10.1093/plankt/fbs070.
Jónasdóttir, S.H., 1999. Lipid content of *Calanus finmarchicus* during overwintering in the Faroe-Shetland Channel. Fish. Oceanogr. 8, 61–72. https://doi.org/10.1046/j.1365-2419.1999.00003.x.
Jørgensen, S.E., Bendoricchio, G., 2001. Fundamentals of Ecological Modelling, vol. 21 Elsevier Science Ltd., Oxford, UK.
Kaartvedt, S., 1996. Habitat preference during overwintering and timing of seasonal vertical migration of *Calanus finmarchicus*. Ophelia 44, 145–156. https://doi.org/10.1080/00785326.1995.10429844.
Kaartvedt, S., 2000. Life history of *Calanus finmarchicus* in the Norwegian Sea in relation to planktivorous fish. ICES J. Mar. Sci. 57, 1819–1824. https://doi.org/10.1006/jmsc.2000.0964.
Kaartvedt, S., Titelman, J., 2018. Planktivorous fish in a future Arctic Ocean of changing ice and unchanged photoperiod. ICES J. Mar. Sci. https://doi.org/10.1093/icesjms/fsx248.
Kane, M.J., Emerson, J.W., Weston, S., 2013. Scalable strategies for computing with massive data. J. Stat. Software 55, 1–19. https://doi.org/10.18637/jss.v055.i14.
Kerfoot, W.B., 1970. Bioenergetics of vertical migration. Am. Nat. 104, 529–546. https://doi.org/10.1086/282688.
Kimmerer, W., McKinnon, A., 1987. Growth, mortality, and secondary production of the copepod *Acartia tranteri* in Westemport Bay, Australia. Limnol. Oceanogr. 32, 14–28. https://doi.org/10.4319/lo.1987.32.1.0014.
Kiørboe, T., 2011. What makes pelagic copepods so successful? J. Plankton Res. 33, 677–685. https://doi.org/10.1093/plankt/fbq159.
Kosobokova, K.N., 1999. The reproductive cycle and life history of the Arctic copepod *Calanus glacialis* in the White Sea. Polar Biol. 22, 254–263.
Kralj-Fišer, S., Schuett, W., 2014. Studying personality variation in invertebrates: why bother? Animal Behav. 91, 41–52. https://doi.org/10.1016/j.anbehav.2014.02.016.
Lampert, W., 1989. The adaptive significance of diel vertical migration of zooplankton. Funct. Ecol. 3, 21–27. https://doi.org/10.2307/2389671.
Langbehn, T.J., Varpe, Ø., 2017. Sea-ice loss boosts visual search: fish foraging and changing pelagic interactions in polar oceans. Global Change Biol. 23, 5318–5330. https://doi.org/10.1111/gcb.13797.
Lee, H.-W., Ban, S., Ikeda, T., Matsuishi, T., 2003. Effect of temperature on development, growth and reproduction in the marine copepod *Pseudocalanus newmani* at satiating food condition. J. Plankton Res. 25, 261–271. https://doi.org/10.1093/plankt/25.3.261.
Lee, R.F., Hagen, W., Kattner, G., 2006. Lipid storage in marine zooplankton. Mar. Ecol. Progr. Series 307, 273–306. https://doi.org/10.3354/meps307273.
Lie, U., 1965. Quantities of zooplankton and propagation of *Calanus finmarchicus* at permanent stations on the Norwegian coast and at Spitsbergen, 1959–1962. Fiskeridirektoratets skrifter, Serie Havundersøkelser 13, 5–19.
Loose, C.J., Dawidowicz, P., 1994. Trade-offs in diel vertical migration by zooplankton: the costs of predator avoidance. Ecology 75, 2255–2263. https://doi.org/10.2307/1940881.
Lorenzen, C.J., 1972. Extinction of light in the ocean by phytoplankton. ICES J. Mar. Sci. 34, 262–267. https://doi.org/10.1093/icesjms/34.2.262.
Lucasius, C.B., Kateman, G., 1989. Application of genetic algorithms in chemometrics. In: Proceedings of the Third International Conference on Genetic Algorithms. Morgan Kaufmann Publishers Inc., pp. 170–176.
Madsen, S.J., Nielsen, T.G., Hansen, B.W., 2001. Annual population development and production by *Calanus finmarchicus*, *C. glacialis* and *C. hyperboreus* in Disko Bay, western Greenland. Mar. Biol. 139, 75–93. https://doi.org/10.1007/s002270100552.
Madsen, S.J., Nielsen, T.G., Tervo, O.M., Söderkvist, J., 2008. Importance of feeding for egg production in *Calanus finmarchicus* and *C. glacialis* during the Arctic spring. Mar. Ecol. Progr. Series 353, 177–190. https://doi.org/10.3354/meps07129.
Mann, K.H., Lazier, J.R.N., 2006. Dynamics of Marine Ecosystems: Biological-Physical Interactions in the Oceans, vol. 3 Blackwell Publishing, Oxford, United Kingdom.
Maps, F., Pershing, A.J., Record, N.R., 2012. A generalized approach for simulating growth and development in diverse marine copepod species. ICES J. Mari. Sci. 69,

370–379. https://doi.org/10.1093/icesjms/fsr182.
Maps, F., Record, N.R., Pershing, A.J., 2013. A metabolic approach to dormancy in pelagic copepods helps explaining inter-and intra-specific variability in life-history strategies. J. Plankton Res. 36, 18–30. https://doi.org/10.1093/plankt/fbt100.
Marshall, S.M., Orr, A.P., 1972. The Biology of a Marine Copepod: Calanus finmarchicus (Gunnerus), vol. 2. Springer Science & Business Media, Berlin, Germany.
Matthews, J.B.L., Hestad, L., Bakke, J.L.W., 1978. Ecological-studies in Korsfjorden, western Norway-generations and stocks of *Calanus hyperboreus* and *Calanus finmarchicus* in 1971–1974. Oceanol. Acta 1, 277–284.
Mauchline, J., 1998. The Biology of Calanoid Copepods, vol. 33 Academic Press, San Diego, California, USA.
McLaren, I.A., 1966. Adaptive significance of large size and long life of the chaetognath *Sagitta elegans* in the arctic. Ecology 47, 852–855. https://doi.org/10.2307/1934273.
McLaren, I.A., Head, E.J.H., Sameoto, D.D., 2001. Life cycles and seasonal distributions of *Calanus finmarchicus* on the central Scotian Shelf. Canadian J. Fish. Aquatic Sci. 58, 659–670. https://doi.org/10.1139/f01-007.
Melle, W., Skjoldal, H.R., 1998. Reproduction and development of *Calanus finmarchicus*, *C. glacialis* and *C. hyperboreus* in the Barents Sea. Mar. Ecol. Progr. Series 169, 211–228. https://doi.org/10.3354/meps169211.
Melle, W., Runge, J.A., Head, E.J.H., Plourde, S., et al., 2014. The North Atlantic Ocean as habitat for *Calanus finmarchicus*: environmental factors and life history traits. Progr. Oceanogr. 129, 244–284. https://doi.org/10.1016/j.pocean.2014.04.026.
Miller, B.L., Goldberg, D.E., 1995. Genetic algorithms, tournament selection, and the effects of noise. Complex Systems 9, 193–212.
Miller, C.B., Crain, J.A., Morgan, C.A., 2000. Oil storage variability in *Calanus finmarchicus*. ICES J. Mar. Sci. 57, 1786–1799. https://doi.org/10.1006/jmsc.2000.0975.
Niehoff, B., Madsen, S.J., Hansen, B., Nielsen, T.G., 2002. Reproductive cycles of three dominant *Calanus species* in Disko Bay, West Greenland. Mar. Biol. 140, 567–576. https://doi.org/10.1007/s00227-001-0731-3.
Ohman, M.D., 1988. Behavioral responses of zooplankton to predation. Bull. Mar. Sci. 43, 530–550.
Parent, G.J., Plourde, S., Turgeon, J., 2011. Overlapping size ranges of *Calanus* spp. off the Canadian Arctic and Atlantic Coasts: impact on species' abundances. J. Plankton Res. 33, 1654–1665. https://doi.org/10.1093/plankt/fbr072.
Pastorok, R.A., 1981. Prey vulnerability and size selection by *Chaoborus* larvae. Ecology 62, 1311–1324. https://doi.org/10.2307/1937295.
Pedersen, G., Tande, K.S., Ottesen, G., 1995. Why does a component of *Calanus finmarchicus* stay in the surface waters during the overwintering period in high latitudes? ICES J. Mar. Sci. 52, 523–531. https://doi.org/10.1016/1054-3139(95)80066-2.
Pepin, P., Head, E.J.H., 2009. Seasonal and depth-dependent variations in the size and lipid contents of stage 5 copepodites of *Calanus finmarchicus* in the waters of the Newfoundland Shelf and the Labrador Sea. Deep Sea Res. Part I: Oceanogr. Res. Papers 56, 989–1002. https://doi.org/10.1016/j.dsr.2009.01.005.
Pijanowska, J., Stolpe, G., 1996. Summer diapause in *Daphnia* as a reaction to the presence of fish. J. Plankton Res. 18, 1407–1412. https://doi.org/10.1093/plankt/18.8.1407.
Plourde, S., Runge, J.A., 1993. Reproduction of the planktonic copepod Calanus finmarchicus in the Lower St. Lawrence Estuary: relation to the cycle of phytoplankton production and evidence for a Calanus pump. Mar. Ecol. Progr. Series 217–227.
Plourde, S., Joly, P., Runge, J.A., Dodson, J., Zakardjian, B., 2003. Life cycle of *Calanus hyperboreus* in the lower St. Lawrence Estuary and its relationship to local environmental conditions. Mar. Ecol. Progr. Series 255, 219–233. https://doi.org/10.3354/meps255219.
Power, M.E., 1992. Top-down and bottom-up forces in food webs: do plants have primacy. Ecology 73, 733–746. https://doi.org/10.2307/1940153.
Pütter, A., 1920. Studien über physiologische Ähnlichkeit VI. Wachstumsähnlichkeiten. Pflüger's Archiv für die Gesamte Physiologie des Menschen und der Tiere 180, 298–340.
R Core Team, 2016. R: A Language and Environment for Statistical Computing. R Foundation for Statistical Computing, Vienna, Austria.
Rardin, R.L., Uzsoy, R., 2001. Experimental evaluation of heuristic optimization algorithms: a tutorial. J. Heuristics 7, 261–304. https://doi.org/10.1023/A:1011319115230.
Record, N.R., Pershing, A.J., Runge, J.A., Mayo, C., Monger, B.C., Chen, C., 2010. Improving ecological forecasts of copepod community dynamics using genetic algorithms. J. Mar. Syst. 82, 96–110. https://doi.org/10.1016/j.jmarsys.2010.04.001.
Renaud, P.E., Berge, J., Varpe, Ø., Lønne, O.J., Nahrgang, J., Ottesen, C., Hallanger, I., 2012. Is the poleward expansion by Atlantic cod and haddock threatening native polar cod, *Boreogadus saida*? Polar Biol. 35, 401–412. https://doi.org/10.1007/s00300-011-1085-z.
Richardson, K., Jónasdóttir, S.H., Hay, S.J., Christoffersen, A., 1999. *Calanus finmarchicus* egg production and food availability in the Faroe-Shetland Channel and northern North Sea: October–March. Fish. Oceanogr. 8, 153–162. https://doi.org/10.1046/j.1365-2419.1999.00007.x.
Robertson, A., 1968. Continuous plankton recorder: a method for studying the biomass of calanoid copepods. Bull. Mar. Ecol. VI, 185–223.
Robledo, L., Soler, A., 2000. Luminous efficacy of global solar radiation for clear skies. Energy Convers. Manage. 41, 1769–1779. https://doi.org/10.1016/S0196-8904(00)00019-4.
Roff, D., 1980. Optimizing development time in a seasonal environment: the 'ups and downs' of clinal variation. Oecologia 45, 202–208. https://doi.org/10.1007/BF00346461.
Rohde, K., 1992. Latitudinal gradients in species diversity: the search for the primary cause. Oikos 65, 514–527. https://doi.org/10.2307/3545569.
RStudio Team, 2016. RStudio: Integrated Development Environment for R. RStudio Inc, Boston, MA, USA.
Runge, J.A., Ingram, R.G., 1991. Under-ice feeding and diel migration by the planktonic copepods *Calanus glacialis* and *Pseudocalanus minutus* in relation to the ice algal production cycle in southeastern Hudson Bay, Canada. Mar. Biol. 108, 217–225. https://doi.org/10.1007/BF01344336.
Sainmont, J., Andersen, K.H., Varpe, Ø., Visser, A.W., 2014. Capital versus income breeding in a seasonal environment. Am. Nat. 184, 466–476. https://doi.org/10.1086/677926.
Sakshaug, E., Johnsen, G.H., Kristiansen, S., von Quillfeldt, C., Rey, F., Slagstad, D., Thingstad, F., 2009. Phytoplankton and primary production. In: Sakshaug, E., Johnsen, G.H., Kovacs, K.M. (Eds.), Ecosystem Barents Sea. Tapir Academic Press, Trondheim, Norway, pp. 167–209.
Scott, C.L., Kwasniewski, S., Falk-Petersen, S., Sargent, J.R., 2000. Lipids and life strategies of *Calanus finmarchicus*, *Calanus glacialis* and *Calanus hyperboreus* in late autumn, Kongsfjorden, Svalbard. Polar Biol. 23, 510–516. https://doi.org/10.1007/s003000000114.
Ślusarczyk, M., 1995. Predator-induced diapause in *Daphnia*. Ecology 76, 1008–1013. https://doi.org/10.2307/1939364.
Smith, S.L., 1990. Egg production and feeding by copepods prior to the spring bloom of phytoplankton in Fram Strait, Greenland Sea. Mar. Biol. 106, 59–69. https://doi.org/10.1007/BF02114675.
Søreide, J.E., Falk-Petersen, S., Hegseth, E.N., Hop, H., Carroll, M.L., Hobson, K.A., Błachowiak-Samołyk, K., 2008. Seasonal feeding strategies of *Calanus* in the high-Arctic Svalbard region. Deep Sea Res. Part II: Topical Stud. Oceanogr. 55, 2225–2244. https://doi.org/10.1016/j.dsr2.2008.05.024.
Søreide, J.E., Leu, E., Berge, J., Graeve, M., Falk-Petersen, S., 2010. Timing of blooms, algal food quality and *Calanus glacialis* reproduction and growth in a changing Arctic. Global Change Biol. 16, 3154–3163. https://doi.org/10.1111/j.1365-2486.2010.02175.x.
Stearns, S., 1989. Trade-offs in life-history evolution. Funct. Ecol. 3, 259–268. https://doi.org/10.2307/2389364.
Stearns, S., Ackermann, M., Doebeli, M., Kaiser, M., 2000. Experimental evolution of aging, growth, and reproduction in fruitflies. Proc. Natl. Acad. Sci. 97, 3309–3313. https://doi.org/10.1073/pnas.97.7.3309.
Strand, E., Huse, G., Giske, J., 2002. Artificial evolution of life history and behavior. Am. Nat. 159, 624–644. https://doi.org/10.1086/339997.
Swalethorp, R., Kjellerup, S., Dünweber, M., Nielsen, T.G., Møller, E.F., Rysgaard, S., Hansen, B.W., 2011. Grazing, egg production, and biochemical evidence of differences in the life strategies of *Calanus finmarchicus*, *C. glacialis* and *C. hyperboreus* in Disko Bay, western Greenland. Mar. Ecol. Progr. Series 429, 125–144. https://doi.org/10.3354/meps09065.
Swift, J.H., 1986. The Arctic Waters. In: Hurdle, B.G. (Ed.), The Nordic Seas. Springer, New York, USA, pp. 129–154.
Szulkin, M., Dawidowicz, P., Dodson, S.I., 2006. Behavioural uniformity as a response to cues of predation risk. Animal Behav. 71, 1013–1019. https://doi.org/10.1016/j.anbehav.2005.05.027.
Tande, K.S., Hopkins, C.C.E., 1981. Ecological investigations of the zooplankton community of Balsfjorden, northern Norway: the genital system in *Calanus finmarchicus* and the role of gonad development in overwintering strategy. Mar. Biol. 63, 159–164. https://doi.org/10.1007/BF00406824.
Tande, K.S., Hassel, A., Slagstad, D., 1985. Gonad maturation and possible life cycle strategies in *Calanus finmarchicus* (Gunnerus) and *C. glacialis* (Jaschnov) in the northwestern part of the Barents Sea. In: Christiensen, M.E. (Ed.), Marine Biology of Polar Regions and Effects of Stress on Marine Organisms. Wiley, Chichester, UK, pp. 141–155.
Tarling, G.A., Burrows, M., Matthews, J., Saborowski, R., Buchholz, F., Bedo, A., Mayzaud, P., 2000. An optimisation model of the diel vertical migration of northern krill (*Meganyctiphanes norvegica*) in the Clyde Sea and the Kattegat. Canadian J. Fish. Aquatic Sci. 57, 38–50. https://doi.org/10.1139/f00-171.
Threlkeld, S.T., 1976. Starvation and the size structure of zooplankton communities. Freshwater Biol. 6, 489–496. https://doi.org/10.1111/j.1365-2427.1976.tb01640.x.
Toivanen, J., Makinen, R.E., Périaux, J., Cloud Cedex, F., 1999. Multidisciplinary shape optimization in aerodynamics and electromagnetics using genetic algorithms. Int. J. Numer. Methods Fluids 30, 149–159. https://doi.org/10.1002/(SICI)1097-0363(19990530)30:2%3C149::AID-FLD829%3E3.0.CO;2-B.
Unstad, K.H., Tande, K.S., 1991. Depth distribution of *Calanus finmarchicus* and *C. glacialis* in relation to environmental conditions in the Barents Sea. Polar Res. 10, 409–420. https://doi.org/10.3402/polar.v10i2.6755.
Varpe, Ø., Fiksen, Ø., Slotte, A., 2005. Meta-ecosystems and biological energy transport from ocean to coast: the ecological importance of herring migration. Oecologia 146, 443. https://doi.org/10.1007/s00442-005-0219-9.
Varpe, Ø., Jørgensen, C., Tarling, G.A., Fiksen, Ø., 2007. Early is better: seasonal egg fitness and timing of reproduction in a zooplankton life-history model. Oikos 116, 1331–1342. https://doi.org/10.1111/j.0030-1299.2007.15893.x.
Varpe, Ø., Jørgensen, C., Tarling, G.A., Fiksen, Ø., 2009. The adaptive value of energy storage and capital breeding in seasonal environments. Oikos 118, 363–370. https://doi.org/10.1111/j.1600-0706.2008.17036.x.
Varpe, Ø., Fiksen, Ø., 2010. Seasonal plankton–fish interactions: light regime, prey phenology, and herring foraging. Ecology 91, 311–318. https://doi.org/10.1890/08-1817.1.
Varpe, Ø., 2012. Fitness and phenology: annual routines and zooplankton adaptations to seasonal cycles. J. Plankton Res. 34, 267–276. https://doi.org/10.1093/plankt/fbr108.
Varpe, Ø., 2017. Life history adaptations to seasonality. Integrat. Comp. Biol. 57, 943–960. https://doi.org/10.1093/icb/icx123.
Visser, A.W., Jónasdóttir, S.H., 1999. Lipids, buoyancy and the seasonal vertical migration of *Calanus finmarchicus*. Fish. Oceanogr. 8, 100–106. https://doi.org/10.1046/j.1365-2419.1999.00001.x.
Vogedes, D., Varpe, Ø., Søreide, J.E., Graeve, M., Berge, J., Falk-Petersen, S., 2010. Lipid sac area as a proxy for individual lipid content of arctic calanoid copepods. J. Plankton Res. 32, 1471–1477. https://doi.org/10.1093/plankt/fbq068.
Von Bertalanffy, L., 1938. A quantitative theory of organic growth (inquiries on growth laws. II). Human Biol. 10, 181–213.

Wells, L., 1970. Effects of Alewife predation on zooplankton populations in Lake Michigan. Limnol. Oceanogr. 15, 556–565. https://doi.org/10.4319/lo.1970.15.4.0556.

Werner, E.E., 1974. The fish size, prey size, handling time relation in several sunfishes and some implications. J. Fish. Board Canada 31, 1531–1536. https://doi.org/10.1139/f74-186.

Williams, C.M., Ragland, G.J., Betini, G., Buckley, L.B., et al., 2017. Understanding evolutionary impacts of seasonality: an introduction to the symposium. Integrat. Comp. Biol. 57, 921–933. https://doi.org/10.1093/icb/icx122.

Zanakis, S.H., Evans, J.R., 1981. Heuristic "optimization": why, when, and how to use it. Interfaces 11, 84–91. https://doi.org/10.1287/inte.11.5.84.

Zaret, T.M., Kerfoot, W.C., 1975. Fish predation on *Bosmina longirostris*: body-size selection versus visibility selection. Ecology 56, 232–237. https://doi.org/10.2307/1935317.

Zaret, T.M., Suffern, J.S., 1976. Vertical migration in zooplankton as a predator avoidance mechanism. Limnol. Oceanogr. 21, 804–813. https://doi.org/10.4319/lo.1976.21.6.0804.